To the Graduate Council:

I am submitting herewith a thesis written by John Alan Howlett entitled "The Sintering Strength of Ash from Potassium Carbonate Seeded Eastern and Western Coals, with a Theory for a Sintering Rate Parameter." I have examined the final copy of this thesis for form and content and recommend that it be accepted in partial fulfillment of the requirements for the degree of Master of Science, with a major in Mechanical Engineering.

Roy J. Schulz

Roy J. Schulz, Ph.D., Major Professor

We have read this thesis
and recommend its acceptance:

John P. [illegible]

Lloyd W. Crawford

Accepted for the Council:

C. W. Minkel

Associate Vice Chancellor
and Dean of The Graduate School

STATEMENT OF PERMISSION TO USE

In presenting this thesis in partial fulfillment of the requirements for a Master's degree at The University of Tennessee, Knoxville, I agree that the Library shall make it available to borrowers under rules of the Library. Brief quotations from this thesis are allowable without special permission, provided that accurate acknowledgement of the source is made.

Permission for extensive quotation from or reproduction of this thesis may be granted by my major professor, or in his absence, by the Head of Interlibrary Services when, in the opinion of either, the proposed use of the material is for scholarly purposes. Any copying or use of the material in this thesis for financial gain shall not be allowed without my written permission.

Signature John Alan Howlett

Date 7 March 1994

THE SINTERING STRENGTH OF ASH FROM POTASSIUM CARBONATE SEEDED EASTERN AND WESTERN COALS, WITH A THEORY FOR A SINTERING RATE PARAMETER

A Thesis

Presented for the

Master of Science

Degree

The University of Tennessee, Knoxville

John Alan Howlett

May, 1994

DEDICATION

This thesis is dedicated to my parents, Mr. and Mrs. John K. Howlett of Kelso, Tennessee, in appreciation of their love, guidance, godly influence, and invaluable education that they have provided me in many facets of life.

ACKNOWLEDGMENTS

I would like to thank my committee members, Dr. Roy Schulz, Dr. John Foote, and Dr. Lloyd Crawford for their valuable assistance throughout this project and my academic tenure. Special thanks is expressed to Mr. Charles Wagoner, my work supervisor, for his patience, kindness, and direction in my work duties and for his contribution to this thesis.

I express my appreciation to Mr. and Mrs. Jeff Fuller of Huntsville, Alabama, who unselfishly and graciously spent many long hours translating a German technical document to assist me. I would like to thank the UTSI laboratory personnel, Philip Sherrill, Kathy Parks, Teresa Young, and John Casey for their assistance in my experiments.

I would also like to thank the family of Temple Baptist Church of Manchester, Tennessee, especially Pastor & Jean Adams, Wayne & Sheila Belew, Ben & Maria Mills, Gary & Cathey Simons, their families, and others who have been an invaluable and wonderful source of Southern hospitality, encouragement, friendship, and assistance in so many ways during my residence. It is my desire that they will not be forgotten.

Finally, but above all, I wish to express my deepest gratitude to the One who has made all possible, my Savior and God, the Lord Jesus Christ, for His undeserved love, His unspeakable gift of eternal salvation, and His presence, all of which He has promised never to take away.

ABSTRACT

This research addresses the strength of coal fly ash deposits on simulated superheater tubes in an U.S. Department of Energy, pilot-scale, coal-fired testing facility called the Coal-Fired Flow Facility (CFFF), operated under magnetohydrodynmamic (MHD) power generation conditions by the University of Tennessee Space Institute. The governing mechanism that develops fly ash deposit strength is sintering. Because deposits on superheater tubes inhibit heat transfer from the flue gas to the tubes, sootblowing is used to remove the ash from the tubes. It is of critical importance to learn more about the relationship between sintering and ash deposit strength, so that sootblower or other ash removal systems may be designed more effectively.

An experimental method was used to examine the relationship between fly ash strength and the sintering process. The method consisted of forming ash pellets at temperatures comparable to those experienced in the exhaust flue gas duct, sintering the pellets at uniform temperature for approximately 15 hours, and crushing the pellets in a compression testing machine. This determined the maximum stress the pellets would withstand, when cold, when they were formed at the given temperature. The research was carried out for two different potassium carbonate seeded coals, an eastern coal, Illinois #6, and a western coal, Montana

Rosebud. Seeded coals are necessary for the coal-fired MHD power generation process.

This research also included an independent derivation of J. Frenkel's model for particle bonding and an application of the model to the specimens used for the crush testing. The size of the bond between ash particles is related to the particle liquidus viscosity and surface tension forces, as well as their sizes. Data required for this part of the research was obtained by photographing the structure of the sintered pellets using a scanning electron microscope (SEM) and by using computer image analysis software to measure the size of the particles and the bonds between them.

Relationships between the strength and the sintering temperature were successfully determined for both eastern and western coal ashes. However, although SEM/computer analysis of the particle bonding was attempted, it was found that, for the time used to heat and sinter the pellets, slagging occurring on the surface and inside the pellet prohibited accurate measurements of bonding, and thus also prohibited finding a reliable correlation between the strength and the sintering rate parameter.

TABLE OF CONTENTS

TABLE OF CONTENTS

LIST OF TABLES

LIST OF FIGURES

LIST OF FIGURES

LIST OF SYMBOLS AND ABBREVIATIONS

CFFF	Coal-Fired Flow Facility
DOE	Department of Energy
MHD	Magnetohydrodynamics
SEM	Scanning Electron Microscope
SHTM	Superheater Test Module
SRP	Sintering Rate Parameter
UTSI	University of Tennessee Space Institute
σ	Surface Tension
ΔS	Change in Surface Area ($S-S_o$)
Φ	Energy dissipated by Viscous Flow
a_o	Original Particle Radius
a	Radius of Particle During and After Bonding
μ	Coefficient of Dynamic Viscosity
Ω_o	Volume of Original Particle System

1 Introduction

1.1 Background of UTSI MHD Research

The University of Tennessee Space Institute (UTSI) has been involved in research and development since it was founded in 1964. One major research effort has been the proof-of-concept testing of coal-fired magnetohydrodynamics (MHD). MHD energy conversion is the conversion of kinetic energy to electrical energy by passing a rapidly flowing, electrically conductive gas through a fixed, high-strength, magnetic field. The gas, a plasma, is created by the combustion of seeded, pulverized coal with oxygen-enriched air. The conductivity of the gas is greatly increased by the addition to the coal of a "seed," often potassium carbonate (K_2CO_3). If used as a "topping cycle" for a conventional steam power plant, the overall efficiency of the plant could be drastically increased, potentially to a level of 50-60%. (Typical coal-fired power plants operate at an efficiency of 32-35%.) See Figure A-1.1 in Appendix A for a schematic layout for a typical MHD power plant.

While research efforts at UTSI in the past have focused on the MHD topping cycle, the "bottoming cycle" is currently the main object of interest. Although the bottoming cycle functions very similarly to a conventional steam power plant in that it involves the production of electrical power using

steam turbines, new problems are introduced by the addition of the seed into the MHD exhaust gas stream. One product of combustion, when the coal contains sulfur in its elemental makeup, is potassium sulfate. The potassium sulfate causes the MHD flue gas to exhibit characteristics somewhat different from those observed previously in conventional plants. Studies on ash deposition, particulate emission, and corrosion in the MHD bottoming cycle have been a major interest and focus in UTSI MHD research.

The Coal Fired Flow Facility (CFFF), located on the UTSI campus and operated under contract to the U.S. Department of Energy (DOE), provides the testing equipment for the MHD research conducted by UTSI personnel. The CFFF simulates a power plant consisting of a boiler, superheater, air heater, baghouse (BH), and electrostatic precipitators (ESP). A drawing describing the layout of the CFFF is shown in Figure A-1.2.

1.2 Background of Problem/Purpose of Study

Of particular interest to this study is the Superheater Test Module (SHTM). The SHTM, although not an actual superheater, is used to investigate superheater performance by operating subject to a flue gas environment that includes temperatures and species that would normally be present in a full-scale MHD superheater. (In a conventional power plant,

the superheater supplies dry or superheated steam to the turbines for power generation.) The SHTM consists of three test sections (containing the steam-cooled simulated superheater tubes) and ten cooling sections containing water-cooled pipes which are used to control the cooling rate of the flue gas. There are eight 2-pass superheater tubes in the first two test sections, eight 4-pass tubes in the third test section, and eight 8-pass or 12-pass tubes in the cooling sections.

As the flue gas flows downstream, it carries ash with it. Some of this ash deposits itself on the superheater tubes, thus inhibiting heat transfer from the gas to the tubes. At gas temperatures normally present in the SHTM, a sintering process takes place, causing the ash particles to bond together and to tube and duct surfaces. The degree of sintering can be described as a function of several parameters, including temperature, time, viscosity, surface tension, chemical composition, and particle size.

Sootblowing is commonly used to attempt to loosen and remove the ash deposits from the superheater tubes. Sootblowing is accomplished by blowing compressed, high-speed air jets onto deposits with the hope of knocking them from the tube surface to which they adhere. However, these systems are not consistently effective on high-strength deposits. A critical need exists to learn more about the relationship between the ash sintering process and deposit

strength so that sootblowing systems may be designed more effectively.

For a given coal with a given chemical composition, it has been shown by Raask [10] that the degree of sintering increases with temperature, at least within some range of temperature. An experimental study of this problem was suggested by Mr. Charles Wagoner, an employee of the UTSI Energy Conversion Programs (ECP) with extensive experience in the coal industry. This study was undertaken in this thesis research to determine the relationships between sintering strength and temperature, for seeded Eastern and Western coal ashes formed when burned under MHD conditions and deposited in the superheater section of the bottoming cycle.

2 Experimental Procedure

During the late 1950's and early 1960's, D.H. Barnhart and Richard Attig [1,2,3,4] employed a method to assess the sintering strength of conventional coal fly ash via cold crushing strength. The method called for forming pellets of fly ash, sintering them at various temperatures ranging from 1500°F-1800°F for a controlled time (15 hours), and crushing them, when cooled to ambient temperatures, to determine the maximum compressive stress they could withstand. The compressive force divided by the cross-sectional area of the pellet was called the sintering strength. This was the

general method used to analyze the strength of MHD fly ash.

2.1 Equipment

The equipment used for the sintering test consisted of the following:

1. Steel die fabricated at UTSI based on the general prototype developed by Attig/Barnhart [1,3]. The dimensions are shown in Figure A-2.1.
2. Steel block used to compress ash, weighing 64 pounds. (The weight of the block is arbitrary, as long as it is heavy enough to compress the ash and that the same weight is used for all pellets.)
3. Aluminum oxide refractory bases.
4. Linberg Sola basic furnace, Type 51441, 4290 Watts.
5. Starrett caliper.
6. Silicon carbide sandpaper.
7. Instron tensile/compression testing machine, Model TTC [6].

2.2 Procedure

The procedure for the experiment is divided into four sections: forming the ash pellet, heating the ash pellet, crushing the ash pellet, and calculating the sintering strength.

2.2.1 Forming of the Ash Pellet Specimens

As-received coal ash, taken from the baghouse of the UTSI CFFF, was placed in the steel die, with care being taken to ensure, as much as possible, an uniform and homogeneous mold. As ash was scooped into the die, the die was shaken and tapped periodically to facilitate the settling of the ash. Also, hand pressure was periodically applied to the piston to further ensure that the ash was settled. When the proper amount of ash was placed into the mold (enough to form a pellet of 0.65 inches diameter and 0.75 inches height in its compressed state), the steel block was used to apply a static load for a period of 30 seconds. This compressed the ash enough to cause the green mold to remain intact as it was ejected onto the refractory base.

2.2.2 Heating the Ash Pellet Specimens

In order to ensure the temperature accuracy of the Linberg furnace, a thermocouple with a Fluke type K digital thermometer was used to obtain a heating curve for the furnace over time. These results were compared with the thermostat set points, and it was found that there existed a constant difference between the thermostat reading and the actual temperature at the pellet location. This correction was used to adjust sintering temperatures.

Since the coal ash was as-received, the pellets had to be dried before being heated at high temperatures to prevent cracking of the pellets. Hence, the thermostat was set to 200°C and the ash was heated at this temperature for one hour. After one hour had elapsed, the thermostat was set to the desired sintering temperature, and, using the heating curve obtained, enough time was given for the furnace to reach the desired temperature before beginning a 15 hour sintering period. After approximately 15 hours, the furnace was turned off, but the door was not opened and the pellets were not removed until at least 24 hours later. The long wait was necessary because early trials showed that the pellets were very susceptible to thermal shock. Some early specimens cracked badly immediately upon being exposed to room temperature, even after cooling slowly in the furnace for approximately eight hours.

2.2.3 Finishing and Crushing the Pellet Specimens

Before the specimens were actually placed in the compression testing machine, silicon carbide paper was used to flatten the ends of the pellets and make them parallel. A caliper was used to make measurements of the height and diameter of the specimen.

After necessary set-up procedures for the compression testing machine were completed, the pellets were mounted in

the machine, using caution to mount them in a manner which prevented eccentric loading. As an extra precaution, fabric tissue (approximately 0.015 inches thick) was placed on the ends. New fabric was used for each specimen.

Using a loading speed of 0.05 inches per minute, the pellet was crushed; and the maximum load applied to the pellet, when the pellet failed, was measured.

2.2.4 Calculating the Sintering Strength

Using the dimensions of the pellet measured by the caliper, the compressive stress (sintering strength) was calculated by dividing the maximum load applied to the pellet by the cross-sectional area. Raw data is reported in Appendix B; however, for the correlation, the arithmetic mean of the compressive stress was used as the sintering strength for specimens heated at each specific temperature.

As the number of samples permitted and as variation made it necessary, outliers (specimens with strength outside ±2 standard deviations) were discarded and a new mean and standard deviation were calculated. This was done because of wide variation in measured strength, which was probably caused by the presence of surface cracks, as discussed in the next section.

3 Results of Sintering Strength Tests

As noted earlier, Attig and Barnhart [1,2,3,4] conducted a series of sintering tests for a wide variety of conventional coal ashes without seed. Examples of some of these curves are given in Figure A-3.1. These coals, all Eastern coals, are noted on the chart by the name of the mine from which they came. Also, in many cases, the boiler type used in the combustion process is noted (P.C. for Pulverized Coal boiler, CYC. for Cyclone boiler, etc.). The results of the experimental work done for this thesis show that the strength of seeded fly ash was, in general, much lower than that of fly ash without seed; however, the general shapes of the curves for the seeded MHD coals were similar to some of those obtained by Attig and Barnhart for the unseeded coals that they used in their experiments.

For the thesis experiments, analysis was done for ash from the combustion of two types of coal that have been used in UTSI MHD tests. One was an ash from a seeded eastern coal, Illinois #6, used in the LMF4 series of CFFF testing. The other was a seeded western coal, Montana Rosebud, used in the LMF5 test series.

Correlation equations were found for each ash that followed the trend of sintering strength versus temperature. It should be noted that for both ashes used in this experiment, the correlations obtained are valid only for the

temperature range of 1400°F-1700°F. The decline in sintering strength above 1700°F would not follow either correlation. There are no correlations available for unseeded coals with which to compare.

Figure A-3.2 is a correlation of the natural log of sintering strength versus the inverse of absolute temperature. Mr. Charles Wagoner suggested attempting this correlation since he theorizes that the degree of sintering is viscously driven, and previous work in the coal industry by Raask [10] has related viscosity of coal ash to the activation energy in the form:

$$\ln(\eta) = \text{Constant} + \frac{E_a}{RT},$$

where η is viscosity, R is the gas constant, and E_a is the activation energy. To this date, no documentation is available that indicates that a relationship between sintering strength and activation energy has ever been established in this manner. However, the good correlation coefficients indicate that a study of this relationship could yield positive results.

3.1 Eastern Coal

An elemental analysis of the raw coal ash content of Illinois #6 coal is listed in Table B-3.1 in Appendix B. The ash used in the experiments was extracted from the baghouse of the UTSI CFFF, and the elemental analysis of this ash is also included in Table B-3.1. The ultimate analysis of the coal is listed in Table B-3.2. The number of specimens tested at each temperature varied somewhat, since some pellets broke during the finishing process before they could be crushed.

As expected, the crushing strength of the ash pellets generally rose with the sintering temperature they experienced, achieving a maximum (on one pellet at 1700°F) of 11,290 psi. However, the strength declined on pellets sintered between 1700°F and 1800°F. Figure A-3.3 is a graph showing the relationship between temperature and sintering strength in analogy to the curves obtained by Attig and Barnhart. (In Figures A-3.3 to A-3.6, the bracketed numbers beside the data points represent the number of specimens tested that were formed at that particular sintering temperature.) Figure A-3.4 presents the correlation equation found to be representative of the behavior of this relationship within the temperature range shown. Table B-3.3 tabulates the raw data obtained for the eastern coal ash.

A problem that presented itself in the calculation of

sintering strength is the effect of surface cracks present on the pellets. Figure A-3.7 is an SEM photograph showing surface cracks. The molten ash exhibited this particular characteristic of ceramics, which, according to common knowledge, greatly influences the strength of the material. Although grinding using a diamond apparatus can be used to smooth the surface and circumvent the problems caused by the cracks, UTSI has no such means to grind ceramics. It is very possible, if not probable, that the presence of these "microcracks" is responsible for the often quite large variation exhibited in the calculated strength. It is also very possible that these cracks were a result of thermal shock; several trials showed that even slow cooling of heated specimens did not always prevent this from happening. Probably this phenomenon would not be present on superheater surfaces due to the very high temperatures that remain fairly constant over long periods of time, although the effects of cool sootblowing air impacting the deposits may contribute to their removal by thermal shock.

3.2 Western Coal

An elemental analysis of raw coal ash content from Montana Rosebud coal is listed in Table B-3.4. The ash used for the thesis experiments came from the baghouse, and its elemental analysis is also listed in Table B-3.4. The

ultimate analysis of the coal is given in Table B-3.5.

There were several observations piquing interest during the series of crushing experiments on Rosebud coal. As expected, again the strength of the ash rose with temperature. Also, the phenomenon of declining strength between 1700°F and 1800°F was observed again. The specimens heated at 1800°F evidenced a melting of some compound in the ash by the formation of a sticky puddle (which hardened during cooling) around and under the pellet. This material was possibly K_2CO_3, which melts at 1644°F. It is possible that the loss of this material from the pellet made a more porous, weaker specimen. Sintering hardly occurred at low temperatures (1400°F and 1500°F). Although a value was obtained for the loads applied at these temperatures, it is very possible that the compression tester is inaccurate at these low ranges. Figure A-3.5 shows a curve analogous to the curves developed by Attig/Barnhart, and Figure A-3.6 is the correlation found that describes the relationship between sintering strength and temperature for the temperatures shown. Tabulated raw data is listed in Table B-3.6.

There were other points of interest. The sintered western coal pellets were extremely hygroscopic, gathering moisture and beginning to dissolve, while the eastern coal was very stable in this respect. The color of the specimens changed significantly with temperature. At low temperatures, the western ash pellets came out of the furnace a light

green; and at higher temperatures, they came out an ocean blue. At the middle temperature tested, 1600°F, the pellets came out green with blue splotches.

3.3 SEM/Computer Analysis

After the specimens were crushed, a specimen from each temperature group was selected that was considered to be fairly representative of the pellets formed at that temperature. This pellet was used for examination under the scanning electron microscope.

Several features of the physical structure of the specimens were noted that prevented, with a relatively limited sample size, the gathering of accurate data. These features are discussed as follows.

It was noticed upon examination with the SEM that, even after the long sintering time, the degree of sintering inside the pellets was much less than that of the outside surface, indicating a low thermal conductivity. With the exception of a pellet formed at 1400°F, the outside surfaces exhibited a smoothly molten surface texture, like a sheet. SEM photographs were made of the structure just under the surface for measurement purposes.

An SEM photograph was made of each ash before sintering and compared with the photographs made of the crushed pellets. It can be seen that the particles of the ash before

sintering are, for the most part, spherical. (See Figures A-3.8 and A-3.9) Some sintering had already taken place in the MHD duct, which is indicated by the presence of a few bonds. Examination of the crushed pellets shows that the "particles" are much bigger and many random shapes have formed by agglomeration of slagged particles. This makes any confident measurement of these particles and the bonds between them impossible due to the inability to accurately distinguish one particle from another. Some measurements were made of the bonds between particles (or agglomerations resembling particles), and these measurements are listed in Tables B-3.7 and B-3.8.

Using the measurements listed in Appendix B, the Sintering Rate Parameter (the ratio of surface tension/ viscosity, discussed in Section 4) was calculated using an average radius of an ellipse formed by the maximum and minimum radii measured by image analysis software. The results showed the SRP to be fairly constant over the range of temperatures considered; which, if the data were considered reliable, would indicate that the SRP is either temperature independent, or that it reaches an asymptotic value after a period of time. The second alternative is more reasonable, as will be discussed in Section 5. Tables B-3.7 and B-3.8 list the results of these calculations.

4 Frenkel's Equation and the Sintering Rate Parameter

4.1 Background

In 1945, the Russian scientist J. Frenkel published his research on viscous flow of crystalline solids in the Russian Journal of Physics [5]. His research included the mathematical derivation of an equation modeling the process of viscous flow between two identical spherical drops. These drops, initially in contact with each other at one point, will eventually contact each other on a circle with radius y. (Figures A-4.1 and A-4.2) Frenkel derived his equation by equating the work done by surface tension per unit time to the rate of energy dissipation due to viscous flow of the liquid. The final form of his equation was

$$y^2 = \frac{3a\sigma t}{2\mu},$$

where y is the radius of the bond interface, a is the particle radius, t is the time of contact, σ is surface tension, and μ is the coefficient of dynamic viscosity.

The possibility of applying this model to various areas of MHD research is a definite area of interest, the overall objective being to determine coal particle viscosity independent of present methods. One method for measuring

viscosity is by a slag viscometer or some similar apparatus, which is very tedious. Another method is to use regression equations, functions of elemental composition and temperature, determined by empirical means. These regression equations for predicting viscosity are unreliable for several reasons. First, these equations were empirically determined from data at temperatures above the regime of interest encountered in MHD superheater deposits. Extrapolation of these curves to lower temperatures poses a risk, evidenced by the observation that the predictions from existing equations vary quite widely. This can be seen in Figure A-4.4, which is a comparison of viscosity values obtained for an UTSI MHD Test LMF5A slag by two different means. The lower curve is a prediction of viscosity based on the Corrected Urbain equation, developed by Kalmonovitch [7]. The other curve is a prediction based on a curve fit to data measured by Babcock and Wilcox. It can be seen that, in the lower temperature range, the extrapolated curve of the Babcock & Wilcox data shows viscosity to be many orders of magnitude above that predicted by the Urbain Equation. Figure A-4.5 shows a comparison of viscosities for glass spheres obtained by using the Frenkel model and by using the Corrected Urbain equation. This study of glass spheres was done by Kuczynski [8]. Again, there is a wide discrepancy between the two curves. A second reason that an alternative method for measuring viscosity would be desirable is the possibility of a

"boundary layer" existing on the outside of an ash particle with a different chemical composition than the bulk of the particle. Since the boundary layer is generally the active part of the particle in the bonding process, an ash analysis used in a regression equation may not give good results.

4.2 Derivation of the Frenkel Model

Upon re-derivation of Frenkel's theory, it was noted that the result depends upon assumptions as to what stresses are primarily responsible for the viscous dissipation of energy. Although Frenkel did not specifically state his assumptions in his publication, critical analysis of his work seems to indicate that he assumed the following: 1) The flow is incompressible, 2) The dissipation due to dilation dominates the shear dissipation, and 3) There is only one velocity defined in the system. A step-through of his theory follows, with a complete derivation in Appendix D.

As earlier stated, Frenkel began with two identical spherical drops. He showed how the particles would bond by the mechanism of viscous flow. These particles eventually form a coalesced pair with the particles intersecting on a circle of radius y. (Figure A-4.2)

Frenkel derived his model by equating the rate of energy dissipation by viscous flow to the rate of work done by the surface tension forces. The general form for this equality

can be expressed as

$$-\sigma \frac{d\Delta S}{dt} = \Phi , \qquad (1)$$

where σ is surface tension, $d\Delta S/dt$ is the rate of increase of surface area (surface area at the time considered minus the original surface area), and Φ is the rate of energy dissipation by viscous action. The derivation of Frenkel's equation is done by relating the quantities in equation (1) to the geometry of the system.

The quantity $d\Delta S/dt$ was found using the constraint that the total volume of the system, comprised of two initially spherical particles, must remain constant and by assuming that θ is small. Using these observations, the geometry of the system yields

$$\frac{d\Delta S}{dt} = -4\pi a_o^2 \theta \frac{d\theta}{dt} . \qquad (2)$$

To find the rate of energy dissipation, Φ, we need the expression for viscous dissipation per unit volume, ϕ. For incompressible flow, in spherical coordinates, this expression is

$$\phi = 2\mu \left\{ \left(\frac{\partial v_r}{\partial r} \right)^2 + \left(\frac{1}{r} \frac{\partial v_\theta}{\partial \theta} + \frac{v_r}{r} \right)^2 + \left(\frac{1}{r \sin \theta} \frac{\partial v_\varphi}{\partial \varphi} + \frac{v_r}{r} + \frac{v_\theta \cot \theta}{r} \right)^2 \right\}$$
$$+ \mu \left\{ \left[r \frac{\partial}{\partial r} \left(\frac{v_\theta}{r} \right) + \frac{1}{r} \frac{\partial v_r}{\partial \theta} \right]^2 + \left[\frac{1}{r \sin \theta} \frac{\partial v_r}{\partial \varphi} + r \frac{\partial}{\partial r} \left(\frac{v_\varphi}{r} \right) \right]^2 \right\}$$
$$+ \mu \left[\frac{\sin \theta}{r} \frac{\partial}{\partial \theta} \left(\frac{v_\varphi}{\sin \theta} \right) + \frac{1}{r \sin \theta} \frac{\partial v_\theta}{\partial \varphi} \right]^2 , \quad (3)$$

where μ is the coefficient of a Newtonian fluid dynamic viscosity. The expression for viscous dissipation is then

$$\Phi = \phi \Omega_o, \quad (4)$$

where Ω_o is the original system volume, which remains constant. Substitution of (3) into (4), and using only the first term in Φ as the primary velocity gradient component responsible for the viscous dissipation, we get

$$4\pi a_o^2 \sigma\theta \frac{d\theta}{dt} = 2\mu \left(\frac{\partial v_r}{\partial r} \right)^2 \Omega_o . \quad (5)$$

Substituting the expression for volume gives:

$$4\pi a_o^2 \sigma\theta \frac{d\theta}{dt} = 2\mu \left(\frac{\partial v_r}{\partial r} \right)^2 \left[2\left(\frac{4}{3}\right)\pi a_o^3 \right]. \quad (6)$$

Simplifying, we obtain

$$\sigma\theta \frac{d\theta}{dt} = \frac{4}{3} a_o \mu \left(\frac{\partial v_r}{\partial r} \right)^2 . \quad (7)$$

The only velocity defined (by Frenkel) is that of the interface as it moves toward the center of the drop. (Figures

A-4.2 and A-4.3) Therefore, the velocity gradient is found to be the ratio

$$\frac{\partial v_r}{\partial r} = a\theta \frac{d\theta}{dt} . \qquad (8)$$

After substitution of equation (8) in equation (7), equation (7) becomes, since $a \approx a_o$,

$$\theta \, d\theta = \frac{3\sigma}{4a_o\mu} dt . \qquad (9)$$

Integrating,

$$\frac{\theta^2}{2} = \frac{3\sigma}{4a_o\mu} t + C_1 . \qquad (10)$$

The integration constant C_1 can be found by applying the initial condition that $\theta=0$ at $t=0$; therefore, C_1 is equal to zero, and

$$\theta^2 = \frac{3\sigma}{2a_o\mu} t . \qquad (11)$$

Since $\sin \theta \approx y/a$; and, in small angle theory, $\sin \theta = \theta$ and $a=a_o$,

$$\theta = \frac{y}{a} ,$$

and substitution yields

$$y^2 = \frac{3\sigma a t}{2\mu} . \qquad (12)$$

The implications of this model are obvious. First, if measurements of the bond radius and particle radius can be made, the value of the viscosity, μ, can be found if surface

tension, σ, is known, or the ratio of σ/μ can be found without having to know elemental composition and temperature. Also, this method does not involve extrapolation of empirical equations into temperature ranges for which they were not intended. The quantity σ/μ, which can be solved for as

$$\frac{\sigma}{\mu} = \frac{2y^2}{3at}, \qquad (13)$$

will be hereafter called the Sintering Rate Parameter, or SRP. This quantity is useful in research on slag buildup on superheater tubes because it can be used to define the propensity of a given particle to "stick" to the surface that it impacts. It is thought that efforts to model the deposition of ash on tubes will eventually make use of this quantity.

It should be noted again that this model was derived assuming that there is only one velocity defined in the system and that the shear terms in the viscous dissipation function are negligible. There is, however, reasonable doubt that these assumptions are completely valid. Frenkel seems to assume, since the volume of the system must remain constant, that the mass displaced flows over the outside layer of each particle evenly, keeping the original shape of the sphere (except for the interface). If this is true, it seems reasonable that shear dissipation exists as the displaced material flows over the outside surface. It is

probably a profitable study to write a Navier-Stokes type computer analysis to study this system and to determine if Frenkel's assumptions are, in fact, justified.

G.C. Kuczynski [8] used Frenkel's method to estimate the viscosity of glass particles. However, certain questions must be answered before this method can be used reliably for coal ash. The first question regards the use of the expression for viscous dissipation, Φ, in particular the use of μ for coal ash, which might not be accurately approximated as a Newtonian fluid at low temperatures. Also, Frenkel's equation was based on the assumption that the two particles were identical and spherical, which in real life, rarely happens. Still a third question concerned the universal application of the small angle theory in the derivation. As the size of the bond increases, the assumption that θ is small is not accurate.

Consequently, it became desirable to develop a method, computational if necessary, to eliminate the stipulation of small angles and identical spherical particles in the analysis. Also, the ability to use this method on non-spherical particles was an area of interest if proven that it could be done.

4.3 Numerical Analysis of Non-spherical Particles and Spherical Particles of Different Sizes

Using the same basic principles stated above, two simple FORTRAN programs were written for the purpose of: 1) finding the ratio of surface tension/viscosity (Sintering Rate Parameter) for two spherical particles of different radii; and 2) determining the feasibility of approximating ellipsoidal particles as spherical particles for use with the Sintering Rate Parameter. The first program analyzed the situation when two ellipsoids were formed by rotating two ellipses about their major axes and subsequently placed in contact on the ends of their major axes. The second program examined the scenario when two ellipsoids formed by rotating ellipses about their minor axes were placed in contact on the ends of their minor axes. (Figure A-4.6) Although, these programs were mainly designed for the purpose of determining whether it was possible to approximate two ellipsoids as two spheres for use in Frenkel's model, the ability to analyze two spheres (or ellipsoids) of different dimensions was included in both programs.

As noted earlier, the same basic engineering principles were used for the FORTRAN programs as were used for the derivation of the Frenkel model. The main difference came in the higher complexity of the mathematics. For example, for ellipsoids, it was necessary to use the formula for surface area of a solid formed by rotating a function about the x-

axis:

$$S = 2\pi \int r(x) \sqrt{[1 + (f'(x))^2]}\, dx ,$$

where r(x) is the distance of the function from the x-axis, and f'(x) is the first derivative of the function.

The programs were written to calculate the Sintering Rate Parameter as the bond interface grew until the maximum or sintering time was reached. A listing of the programs is included in Appendix C.

4.4 Computer Program Results

A list of sample results is included in Tables C-4.1 and C-4.2 in Appendix C. Various dimensions were used that would test the accuracy of the programs for non-spherical particles and spherical particles of different dimensions. By using values close to that of identical spheres, it was seen that the programs do have reasonable accuracy. An example is given with dimensions that will give a large angle in Frenkel's model. The results show the inaccuracy obtained when this angle is treated as small in Frenkel's equation. Also, as can be seen from the sample input/output listing, the SRP stayed essentially constant until the complete sintering time was expired. This is the expected result.

Another interesting observation is that, generally, non-

spherical particles can be approximated as spherical particles if only the order of magnitude of the SRP is wanted. However, the exact value deviates as the shape tends farther from a sphere. Also, of course, different results are obtained with each program depending on how the ellipsoids are placed in contact. This also is shown by the list of results. However, the use of the programs to find the SRP for two spherical particles with different radii seems to be justified.

5 Conclusions and Recommendations

5.1 Conclusions

Several observations can be made from the data as it relates to the overall scope of this thesis.

The first and most obvious conclusion concerns the comparative strengths of the two ashes. A western coal ash is seen to be much weaker than eastern ash sintered at the same temperature. Photographs also show its structure to contain less slagging. The western pellets, especially those formed at lower temperatures, were "powdery" when taken from the furnace, which is consistent with what is found in the MHD duct after tests. Unfortunately, there is no significant or well-developed data base for the relationship between ash chemistry and strength; however, it is theorized herein that

the difference in chemical makeup is predominately responsible for the difference in strength between the eastern and western coals.

The second conclusion relates to the ability to use Frenkel's model for measuring the Sintering Rate Parameter. As was mentioned before, it was impossible to get meaningful measurements under the test conditions imposed by the experiments. If the data collected were interpreted literally, it would indicate that the Sintering Rate Parameter has no temperature dependency in the range of temperature examined, and that the SRP was fairly constant for all specimens crushed. However, previous research in the coal industry seems to indicate otherwise. It is much more reasonable that the SRP approached an asymptotic value due to the very long sintering time of the pellets. Although it may be possible that the SRP is a weak function of temperature within this range, again, previous work in the coal industry indicates the exact opposite. Another possible implication is that the surface of coal fly ash cannot be classified as a Newtonian fluid at these temperatures, possibly making Frenkel's model inapplicable. However, it may be possible that this method and Frenkel's model can be useful if test conditions are implemented for shorter sintering times, which would reduce surface slagging and internal multi-particle agglomerations.

A definite advantage of this method, if it is modified,

is the ability to make measurements of the SRP with a small amount of material. Conversely, slag viscometers usually require approximately 150 grams per measurement.

5.2 Recommendations

Very obviously, all other parameters being equivalent, seeded western coal, from the deposition removal standpoint, seems to be the desirable fuel to burn for ash removal purposes in coal-fired MHD power plants. However, depending on the temperature present at the location under consideration, the deposit strength may still be too high to completely, effectively remove such deposits with compressed air from a sootblower. To this date, the relationship between cold and hot strength is uncertain.

This suggests that alternative methods to removing deposits should be considered in more depth. One possible mechanism would be the low thermal conductivity evidenced by the ash deposits. It was noticed in the early stages of testing that the pellets were extremely susceptible to thermal shock. If this property could be exploited without causing damage to the structure on which the deposit rests, this could be a very effective way of removing the deposits. To this date, such a method has not been found.

Another avenue to consider revolves around the tendency of the ash deposits to decrease strength at higher

temperatures. (This phenomenon was also noted in unseeded coals tested by Attig and Barnhart [3].) It is possible that a chemical breakdown of some sort occurs at high temperatures. In the event that this process could be accelerated or controlled chemically or by other means, this might decrease strength enough to make sootblowing a more reasonable alternative.

Other recommendations can be made concerning the measurement of the Sintering Rate Parameter and its attempted correlation to sintering strength. Some major modifications of this procedure are necessary. As indicated earlier, slagging of the particles on the surface and within the pellets prevented accurate measurement of particle bonding within the pellets themselves. A possible modification to the experiment would be to continue the Attig/Barnhart procedure for measuring sintering strength, but measure the SRP from separate samples of the same ash heated to the same temperature for much shorter periods of time, perhaps one to four hours, depending on iteration for each ash. Furthermore, the ash for measuring the SRP need not be tightly compressed in a large pellet, preventing complete sintering throughout the pellet, but instead could be much looser since the size of the particles facilitates particle contact. Heating for shorter periods of time will keep the particles from losing their identity and keep the size of the bonds much lower, making procurement of better data much more

possible. A correlation could then be made between the SRP and the sintering strength, which was initially one of the desired goals for this experiment.

Another recommendation would be to "classify," if possible, the particles into different categories based on their diameters. Having particles of similar size reacting together would probably prevent some of the smaller size particles from losing their geometric identity as they flow into other comparatively large particles. They do not, however, have to be identically sized to measure the Sintering Rate Parameter, since the FORTRAN programs listed in Appendix C have the capability of analyzing the more diverse bonding situations experienced in nature.

BIBLIOGRAPHY

BIBLIOGRAPHY

[1] Attig, R.C., "Development of a Coal Ash Fouling Index Based on Laboratory Ashing Furnace Tests, Research Center Report 7793," Alliance, OH: Babcock & Wilcox Research Center, 1967.

[2] Attig, R.C., "Progress Report No. 1, Ash Characteristics as Related to Boiler Cleaning Requirements, RDE-1122, Research Report No. 4304," Alliance, OH: Babcock & Wilcox Research Center, 1960.

[3] Barnhart, D.H., "Research on Coal-Ash Characteristics as Related to the Boiler Cleaning Problem, Report No. 7400," Alliance, OH: Babcock & Wilcox Research Center, 1961.

[4] Ely, F.G. and Barnhart, D.H., "Coal Ash--Its Effect on Boiler Availability," Alliance, OH: Babcock & Wilcox Research Center, 1961.

[5] Frenkel, J., "Viscous Flow of Crystalline Bodies Under the Action of Surface Tension," Russian Journal of Physics, 1945.

[6] Instron Models TT-B & TT-C Testing Instruments, Instron Corporation, 1964.

[7] Kalmonovitch, D.P. and Frank, M., " An Effective Model of Viscosity for Ash Deposition Phenomena," Proc. Engineering Foundation Conference on Mineral Matter and Ash Deposition from Coal, ed. by R.W. Byers and K.S. Vorres, Santa Barbara, CA: United Engineering Trustees, Inc., 1990.

[8] Kuczynski, G.C., "Study of the Sintering of Glass," Journal of Applied Physics, 1949.

[9] MHD Program Plan, U.S. Department of Energy, Washington, D.C.: U.S. Department of Energy, 1990.

[10] Raask, Erich, Mineral Impurities in Coal Combustion, Washington, D.C.: Hemisphere Publishing Corporation, 1985.

APPENDICES

APPENDIX A

(FIGURES)

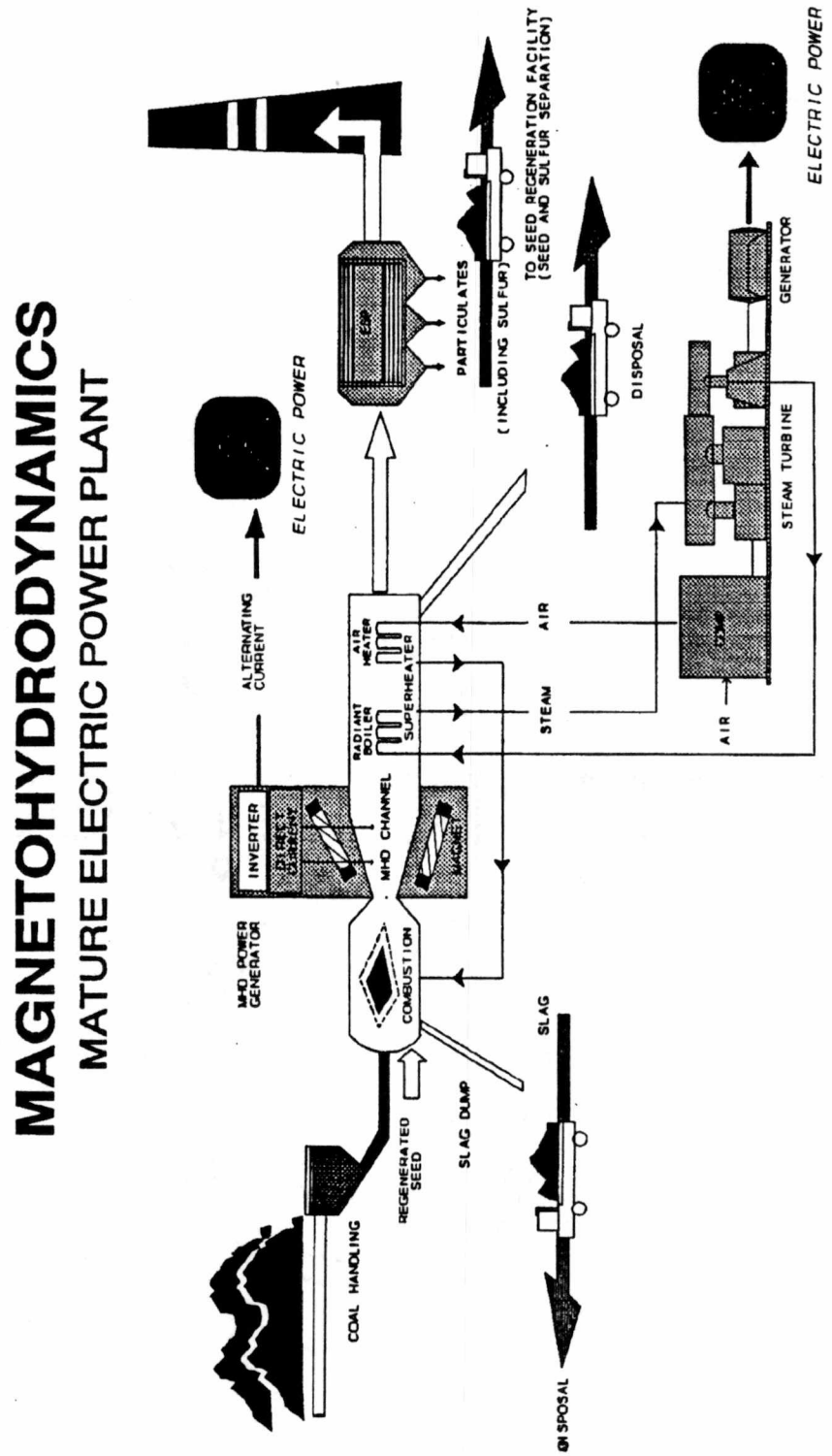

Figure A-1.1 General Layout of MHD Power Plant [9]

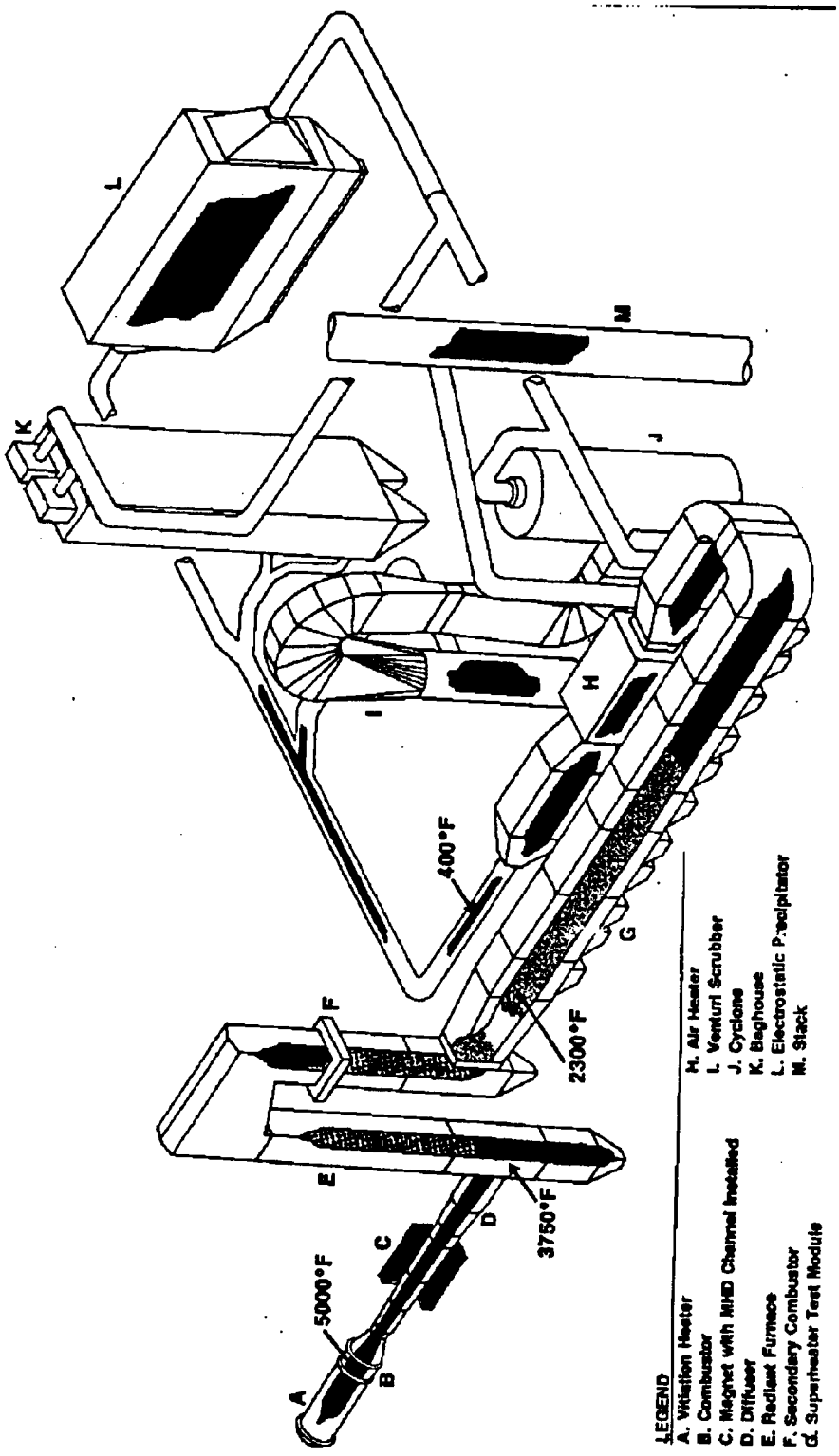

Figure A-1.2 Layout of UTSI Coal-Fired Flow Facility

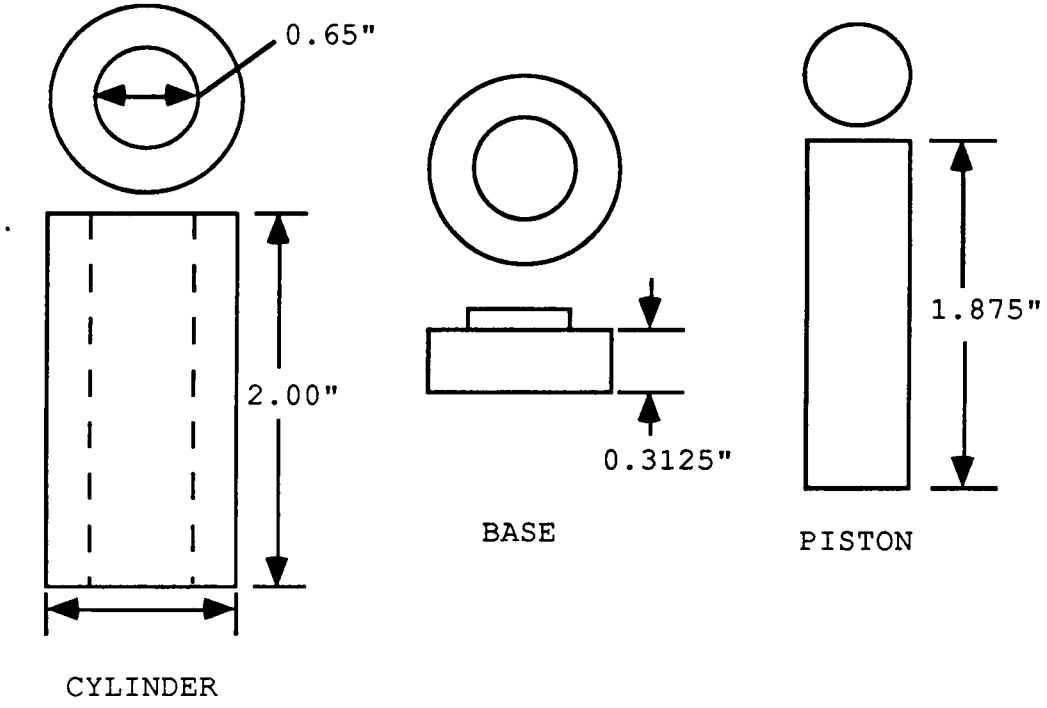

Figure A-2.1 Mold Assembly

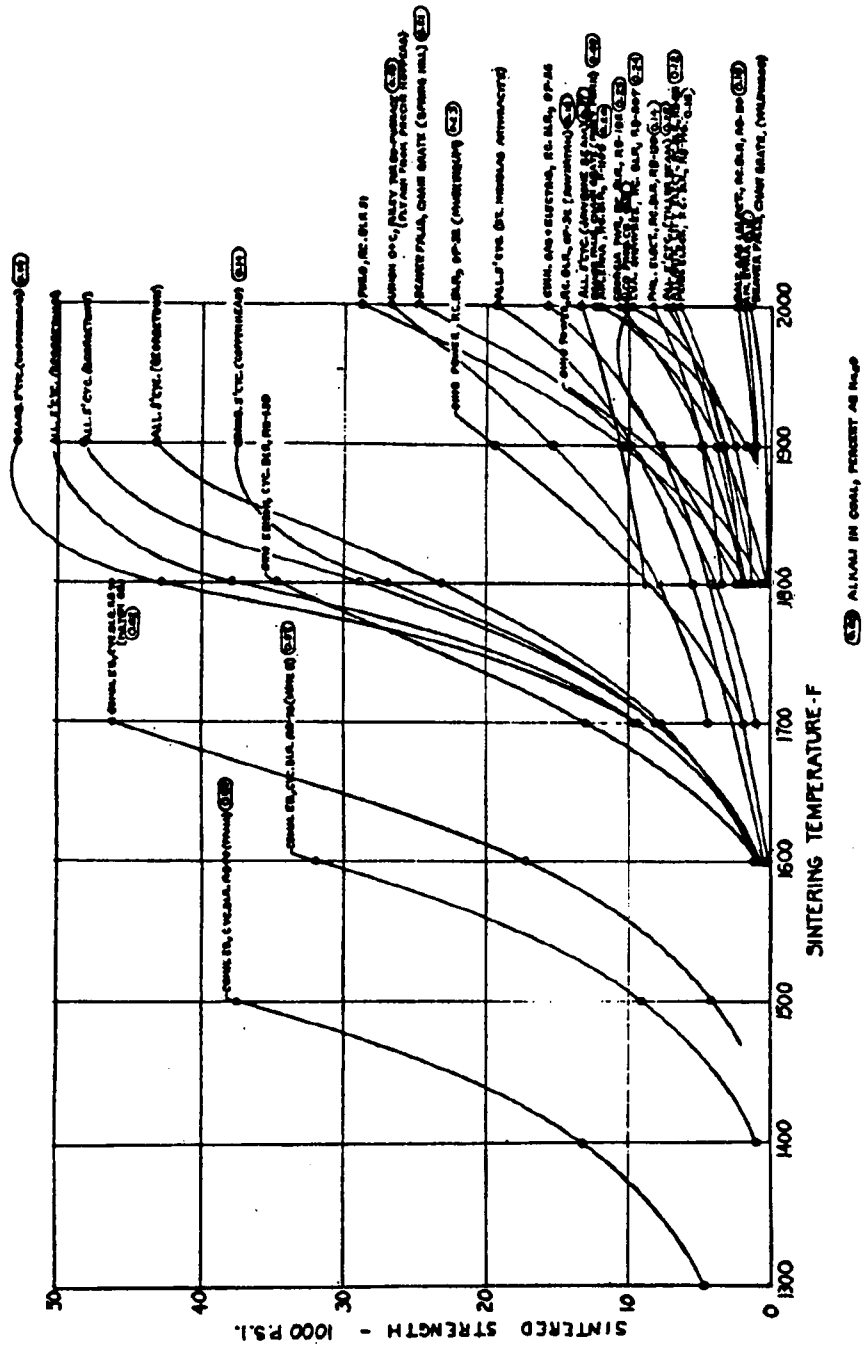

Figure A-3.1 Examples of Curves of Sintering Strength Versus Temperature for Unseeded Coals, Tested by Attig and Barnhart [3]

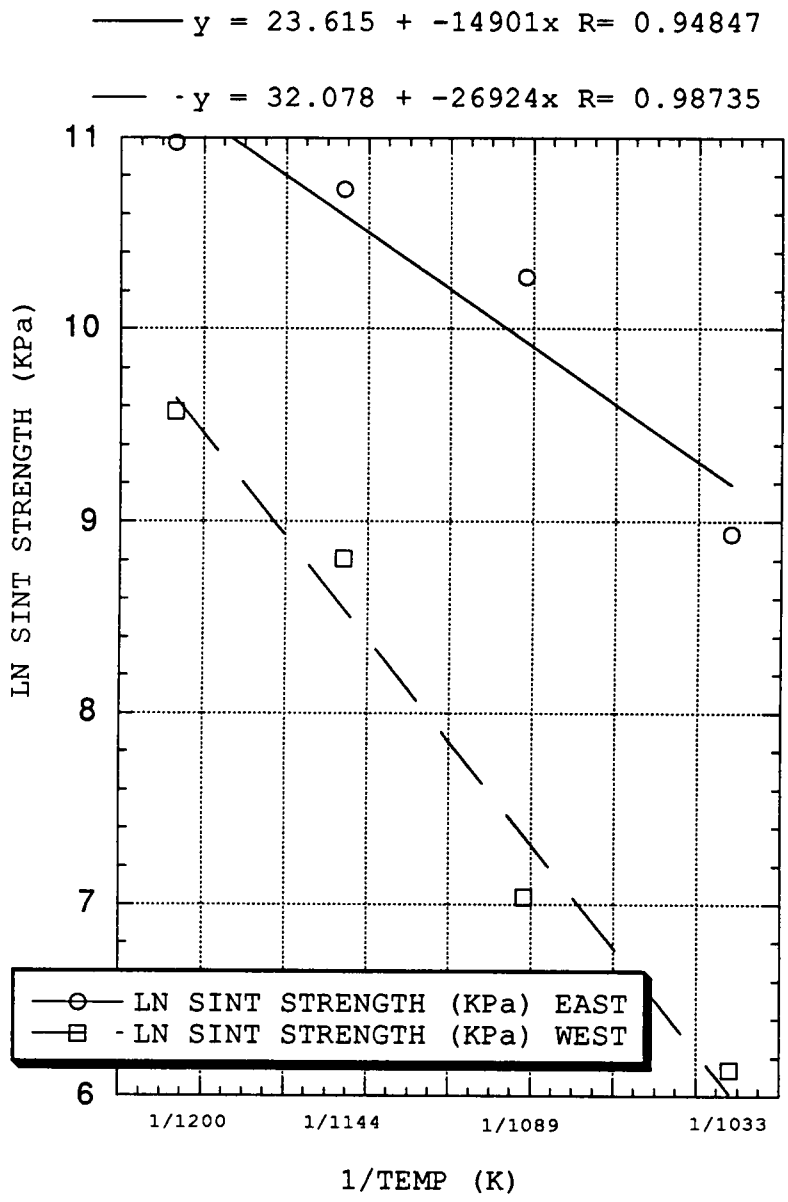

Figure A-3.2 Comparison of the Natural Log of Sintering Strength Versus the Inverse of Temperature for Eastern and Western Coal Ashes

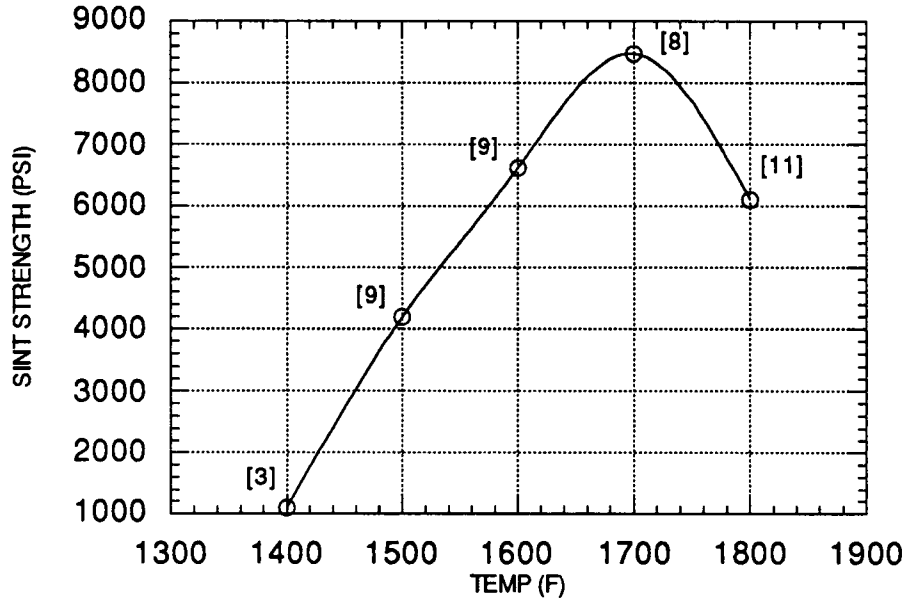

Figure A-3.3 Sintering Strength Versus Sintering Temperature of Seeded Illinois #6 Coal Ash, Extracted from the Baghouse of the U.S. Department of Energy Coal-Fired Flow Facility

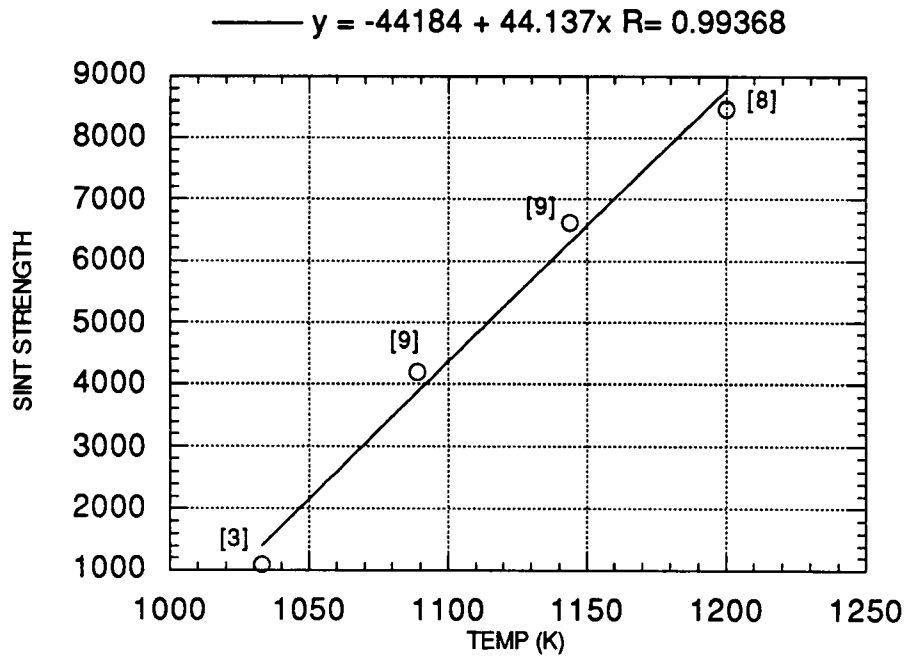

Figure A-3.4 Correlation of Sintering Strength Versus Temperature for Illinois #6 Coal Ash

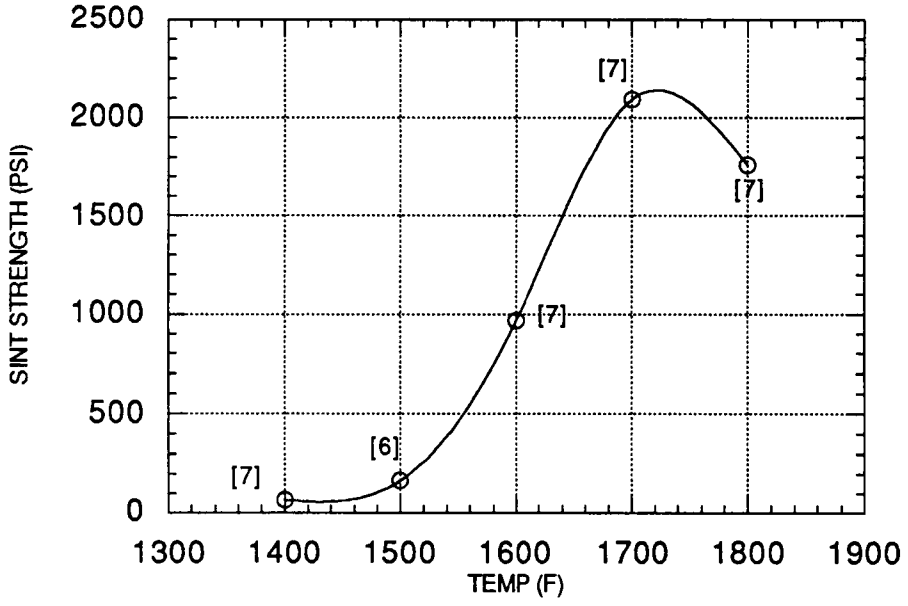

Figure A-3.5 Sintering Strength Versus Sintering Temperature of Seeded Montana Rosebud Coal Ash, Extracted from the Baghouse of the U.S. Department of Energy Coal-Fired Flow Facility

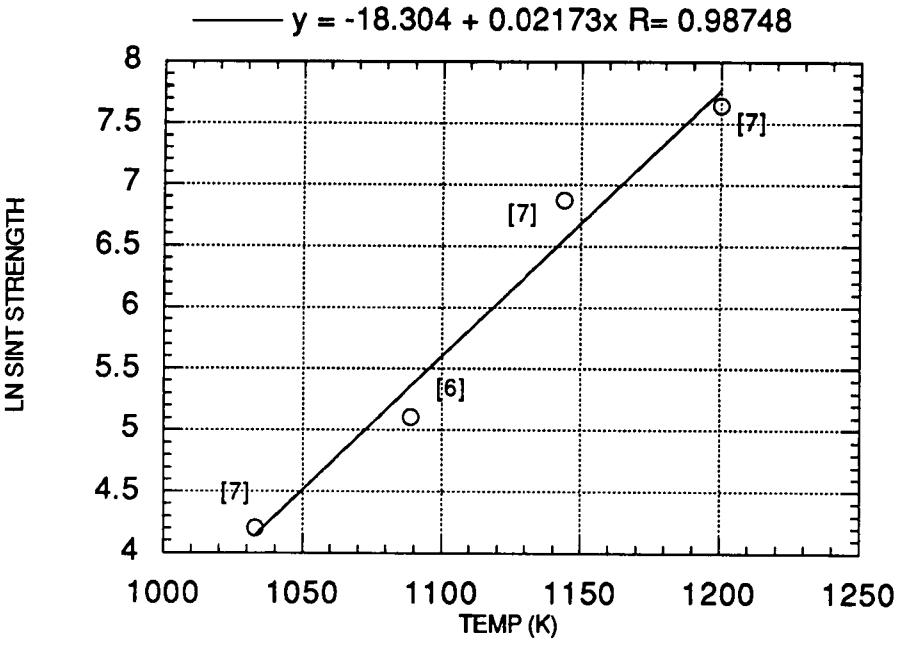

Figure A-3.6 Correlation of Sintering Strength Versus Temperature for Montana Rosebud Coal Ash

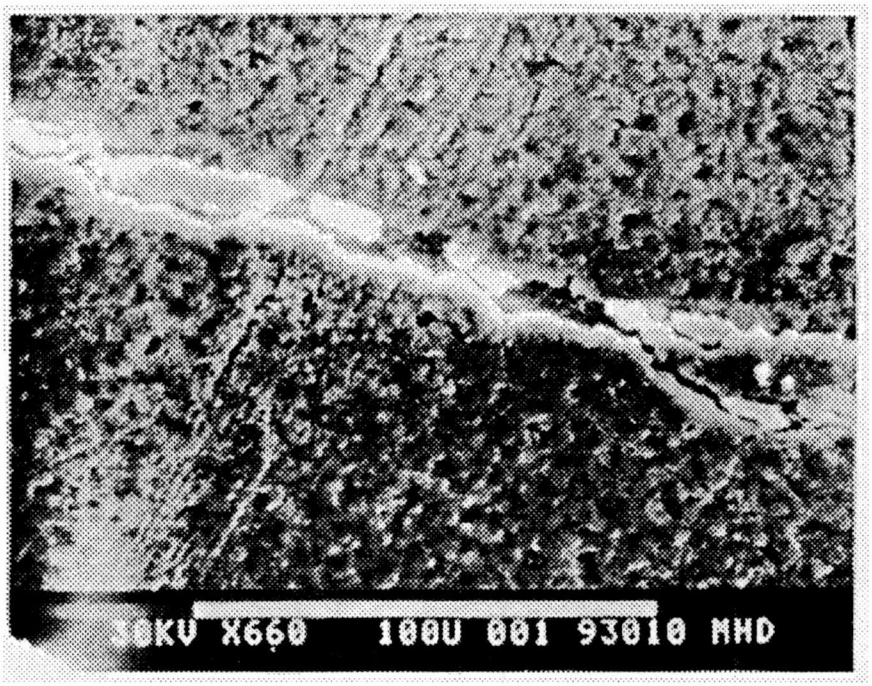

Figure A-3.7 SEM photograph showing surface cracks on surface of pellet

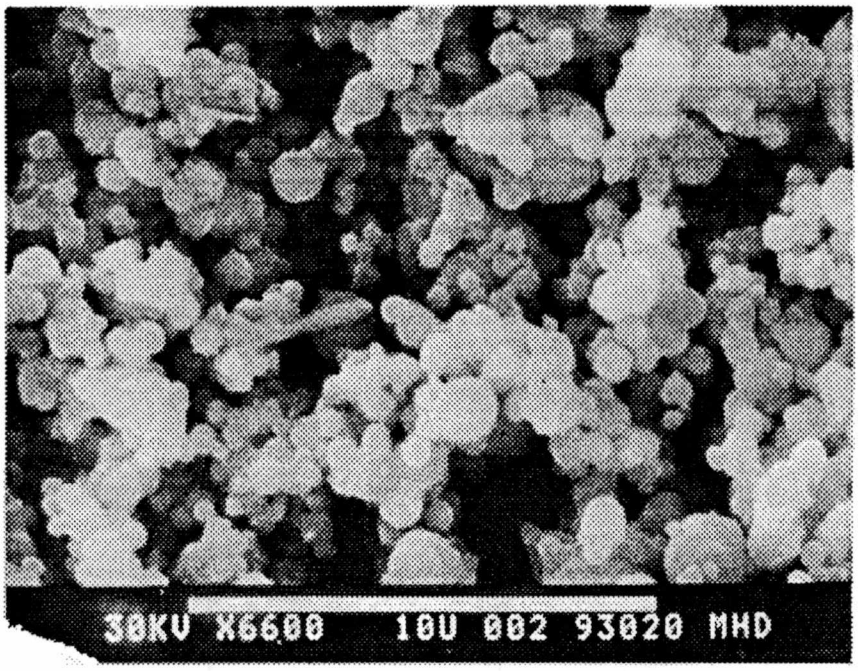

Figure A-3.8 SEM Photograph of Eastern Fly Ash Before Sintering Test

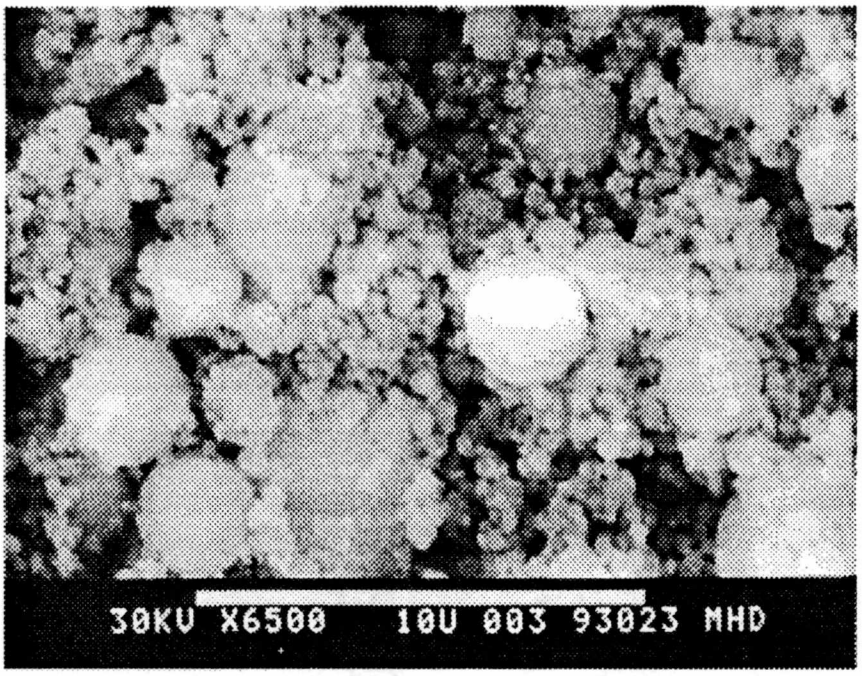

Figure A-3.9 SEM Photograph of Western Fly Ash Before Sintering Test (Microscope technical problems prevented a good picture.)

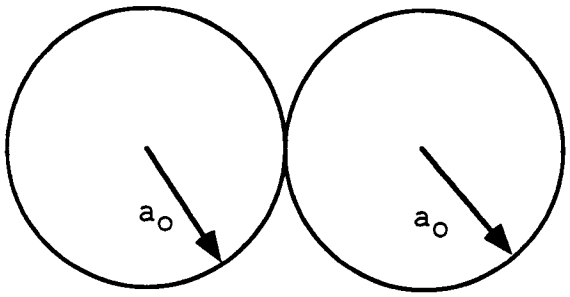

Figure A-4.1 Frenkel's Original Particle System

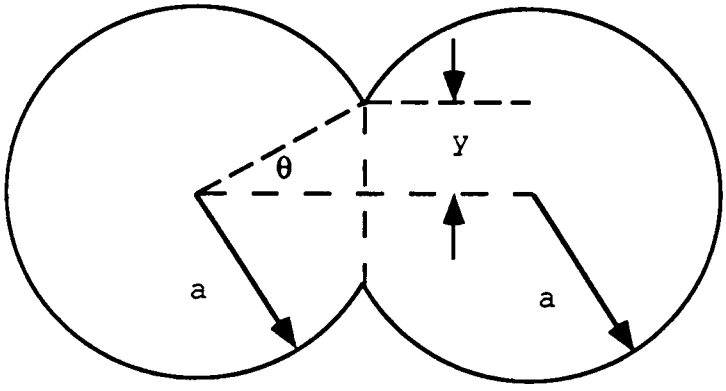

Figure A-4.2 Frenkel's System During Bonding

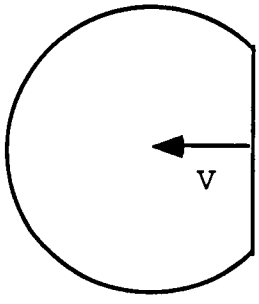

Figure A-4.3 Velocity Defined in the Frenkel Derivation

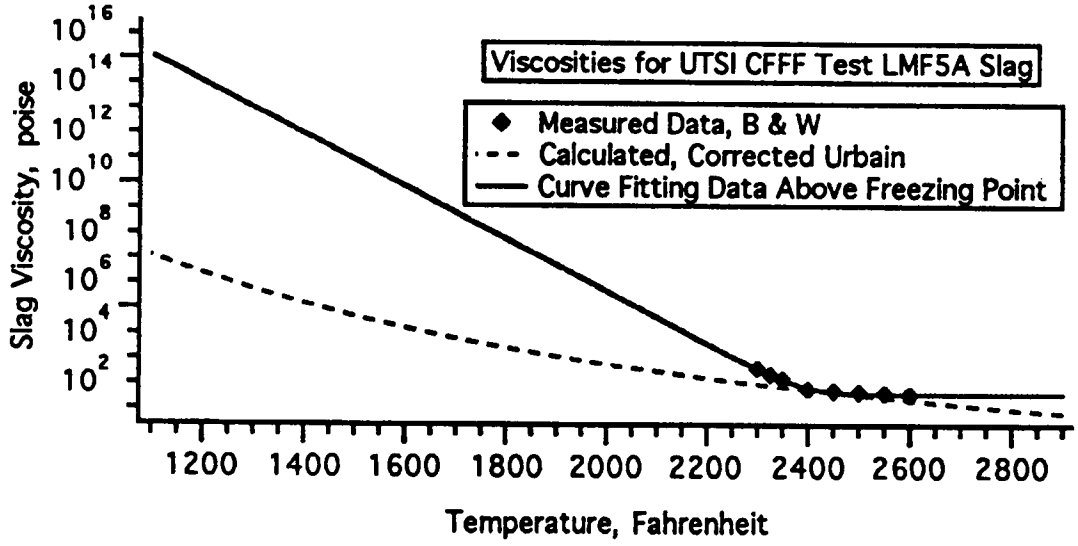

Figure A-4.4 Comparison of Viscosity Measurements by Babcock & Wilcox and Correlation Predictions for an UTSI CFFF Test LMF5A Slag

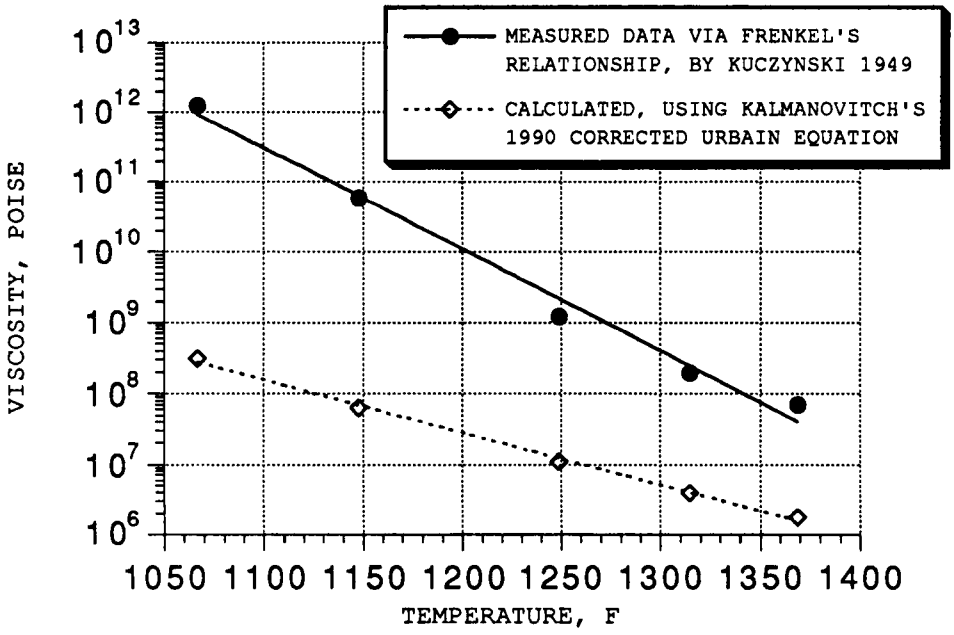

Figure A-4.5 Comparison Between Viscosity Measurements by Kuczynski [8] Using Frenkel's Model Versus Correlation Predictions on Glass Spheres

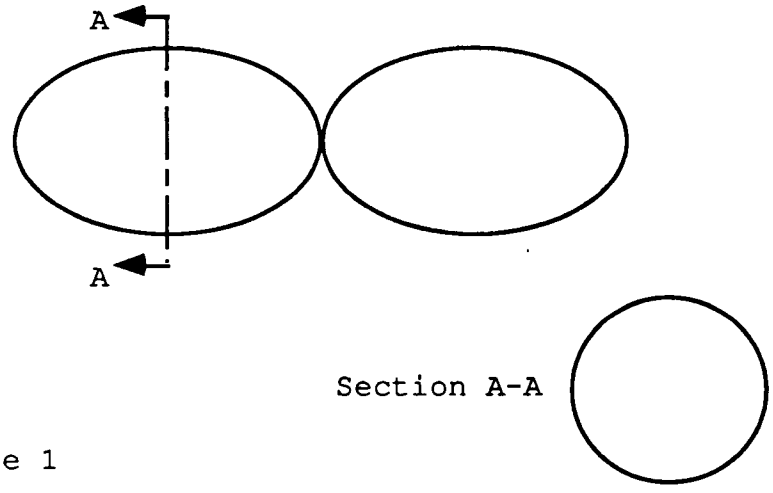

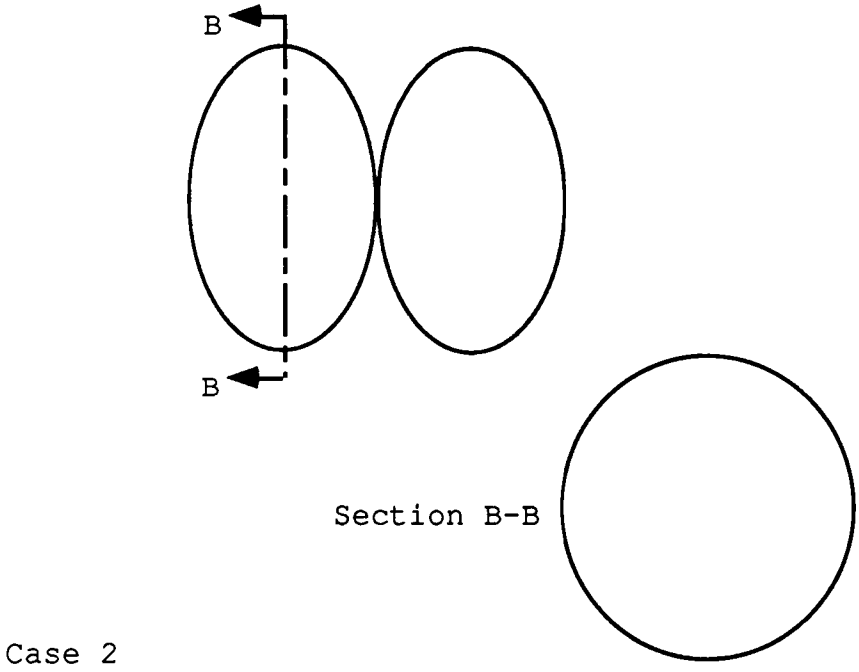

Figure A-4.6 Geometries of the Two Ellipsoidal Particle Configurations Modeled Numerically

APPENDIX B

(TABLES)

Table B-3.1 Mineral Matter Analysis for Illinois #6 Coal

	Raw Coal	Ash
SiO_2	47.9	7.45
Al_2O_3	20.0	2.29
Fe_2O_3	18.7	3.24
TiO_2	0.87	0.30
CaO	2.65	0.37
MgO	0.75	0.12
Na_2O	0.45	0.49
K_2O	6.60	45.74
SO_3	3.15	39.88
Cr_2O_3	NA	0.04
Total	101.07	99.92

Table B-3.2 Ultimate Analysis for Illinois #6 Coal, Dry Basis

Sulfur	3.30
Carbon	68.7
Hydrogen	4.75
Nitrogen	1.30
Oxygen	10.7
Ash	11.3

Table B-3.3 Raw Data/Eastern Coal

Temp. (°F)	Specimen Number	Height (in)	Diameter (in)	Area (sq in)	Load (lb)	Stress (psi)
1400	1	0.510	0.533	0.223	258	1160
	2	0.623	0.546	0.234	276	1180
	3	0.535	0.540	0.229	220	960
	Mean	0.556	0.540	0.229	251	1100
	St. Dev.	0.048	0.005	0.004	23	99
1500	1	0.571	0.509	0.203	982	4840
	2	0.531	0.499	0.196	728	3710
	3	0.565	0.499	0.196	658	3360
	4	0.554	0.507	0.201	1092	5430
	5	0.616	0.513	0.207	900	4350
	6	0.548	0.477	0.179	600	3350
	7	0.544	0.465	0.170	783	4600
	8	0.561	0.474	0.176	684	3890
	9	0.539	0.465	0.170	714	4200
	Mean	0.559	0.490	0.189	793	4190
	St. Dev.	0.024	0.018	0.014	154	656
1600	1	0.558	0.508	0.203	1452	7150
	2	0.572	0.510	0.204	1746	8660
	3	0.550	0.503	0.199	1412	7100
	4	0.534	0.486	0.186	1336	7180
	5	0.532	0.480	0.181	730	4030
	6	0.531	0.477	0.179	1146	6400
	7	0.529	0.475	0.177	914	5160
	8	0.531	0.465	0.170	1414	8320
	9	0.538	0.473	0.176	976	5540
	Mean	0.542	0.486	0.186	1236	6620
	St. Dev.	0.014	0.016	0.012	301	1411

Table B-3.3 Raw Data/Eastern Coal (Continued)

Temp. (°F)	Specimen Number	Height (in)	Diameter (in)	Area (sq in)	Load (lb)	Stress (psi)
1700	1	0.529	0.487	0.186	2200	11290
	2	0.540	0.496	0.193	1580	8190
	3	0.577	0.503	0.199	1370	6880
	4	0.538	0.502	0.198	2165	10930
	5	0.510	0.475	0.177	1145	6470
	6	0.549	0.471	0.174	1785	10260
	7	0.540	0.479	0.180	1500	8330
	8	0.601	0.471	0.174	935	5370
	Mean	0.548	0.486	0.185	1585	8470
	St. Dev.	0.027	0.013	0.010	422	2045
1800	1	0.545	0.510	0.204	1460	7130
	2	0.555	0.487	0.186	880	4730
	3	0.566	0.508	0.202	1140	5620
	4	0.567	0.510	0.204	1780	8370
	5	0.525	0.481	0.182	1010	5550
	6	0.544	0.481	0.182	510	2800
	7	0.550	0.480	0.181	1175	6490
	8	0.540	0.487	0.186	1415	7610
	9	0.564	0.479	0.180	1075	5970
	10	0.545	0.490	0.189	1580	8360
	11	0.526	0.486	0.186	765	4410
	Mean	0.548	0.491	0.189	1163	6100
	St. Dev.	0.014	0.012	0.090	357	1727

Table B-3.4 Mineral Matter Analysis for Montana Rosebud Coal

	Raw Coal	Ash
SiO_2	38.29	9.41
Al_2O_3	17.32	4.43
Fe_2O_3	4.99	1.56
TiO_2	0.81	0.30
CaO	18.86	5.56
MgO	4.38	1.62
Na_2O	0.40	0.56
K_2O	0.57	47.48
SO_3	14.36	18.82
Cr_2O_3	0.04	NA
Carbonate	NA	9.62
Total	100.02	99.36

Table B-3.5 Ultimate Analysis for Montana Rosebud Coal, Dry Basis

Sulfur	0.83
Carbon	65.46
Hydrogen	4.00
Nitrogen	1.48
Oxygen	17.64
Ash	10.59

Table B-3.6 Raw Data/Western Coal

Temp. (°F)	Specimen Number	Height (in)	Diameter (in)	Area (sq in)	Load (lb)	Stress (psi)
1400	1	0.705	0.653	0.335	22	66
	2	0.698	0.653	0.335	24	72
	3	0.741	0.659	0.341	23	72
	4	0.692	0.648	0.330	21	62
	5	0.703	0.643	0.325	22	66
	6	0.708	0.654	0.336	24	73
	7	0.709	0.641	0.323	20	60
	Mean	0.708	0.650	0.332	22	67
	St. Dev.	0.015	0.006	0.006	1	5
1500	1	0.670	0.632	0.314	40	126
	2	0.700	0.625	0.307	54	176
	3	0.701	0.617	0.299	50	167
	4	0.696	0.622	0.304	59	193
	5	0.672	0.624	0.306	57	186
	6	0.694	0.632	0.314	44	139
	Mean	0.689	0.625	0.307	51	165
	St. Dev.	0.013	0.005	0.005	7	24
1600	1	0.647	0.572	0.257	220	856
	2	0.647	0.573	0.258	267	1040
	3	0.667	0.572	0.257	263	1020
	4	0.615	0.565	0.251	234	932
	5	0.620	0.568	0.253	290	1150
	6	0.659	0.588	0.272	251	923
	7	0.710	0.574	0.259	219	846
	Mean	0.652	0.573	0.258	249	967
	St. Dev.	0.029	0.007	0.006	24	101
1700	1	0.612	0.530	0.221	425	1920
	2	0.550	0.521	0.213	427	2010
	3	0.569	0.512	0.206	434	2110
	4	0.584	0.510	0.204	378	1850
	5	0.575	0.508	0.203	470	2320
	6	0.559	0.509	0.203	509	2510
	7	0.577	0.519	0.212	412	1940
	Mean	0.575	0.516	0.209	436	2090
	St. Dev.	0.018	0.007	0.006	39	222

Table B-3.6 Raw Data/Western Coal (Continued)

Temp. (°F)	Specimen Number	Height (in)	Diameter (in)	Area (sq in)	Load (lb)	Stress (psi)
1800	1	0.556	0.485	0.185	308	1670
	2	0.586	0.483	0.183	257	1400
	3	0.533	0.469	0.173	315	1820
	4	0.554	0.479	0.180	338	1880
	5	0.560	0.475	0.177	420	2370
	6	0.570	0.483	0.183	338	1850
	7	0.582	0.484	0.184	247	1340
	Mean	0.563	0.480	0.181	318	1760
	St. Dev.	0.017	0.005	0.004	54	319

Table B-3.7 Data and Calculated SRP for Eastern Ash

Radii are in microns.

	Measured Radii					Average Radii		
Temp.	Particle 1		Particle 2		Bond	1	2	SRP
1400	1.22	1.22	1.37	1.37	0.51	1.22	1.37	0.30E-11
	0.61	0.61	1.07	1.17	0.43	0.61	1.10	0.48E-11
	0.56	0.56	0.36	0.36	0.24	0.56	0.36	0.24E-11
Mean								0.34E-11
1500	0.79	0.79	0.89	0.89	0.46	0.79	0.89	0.44E-11
	1.78	1.78	1.88	1.98	0.94	1.78	1.92	0.80E-11
	0.80	0.90	0.90	0.90	0.60	0.84	0.90	0.90E-11
	1.10	1.10	2.00	1.90	0.86	1.10	1.94	1.08E-11
	1.20	1.10	1.40	1.30	0.78	1.14	1.34	1.00E-11
	0.70	0.70	0.90	0.90	0.42	0.70	0.90	0.40E-11
Mean								0.76E-11
1600	0.84	0.89	0.94	0.89	0.45	0.86	0.91	0.38E-11
	0.99	0.89	0.79	0.79	0.55	0.93	0.79	0.70E-11
	0.99	0.99	0.99	0.89	0.52	0.99	0.93	0.48E-11
	1.09	1.19	1.19	1.09	0.72	1.13	1.13	0.90E-11
	0.79	0.79	0.79	0.79	0.39	0.79	0.79	0.32E-11
	0.66	0.66	0.52	0.52	0.39	0.66	0.52	0.56E-11
Mean								0.56E-11
1700	0.63	0.63	0.44	0.44	0.26	0.63	0.44	0.22E-11
	0.39	0.39	0.54	0.54	0.23	0.39	0.54	0.20E-11
	1.28	1.28	1.38	1.38	0.79	1.28	1.38	0.74E-11
	0.73	0.73	1.18	1.18	0.49	0.73	1.18	0.50E-11
	0.41	0.41	0.36	0.36	0.31	0.41	0.36	0.78E-11
	0.61	0.61	0.61	0.61	0.34	0.61	0.61	0.34E-11
	1.32	1.32	1.42	1.32	0.78	1.32	1.35	0.82E-11
	2.02	2.22	1.32	1.42	0.61	2.09	1.35	0.40E-11
Mean								0.50E-11
1800	1.87	1.94	1.67	1.57	0.90	1.90	1.60	1.08E-11
	1.67	1.67	1.38	1.38	0.89	1.67	1.38	0.96E-11
Mean								0.92E-11

Table B-3.8 Data and Calculated SRP for Western Ash

Radii are in microns.

	Measured Radii					Average Radii		
Temp.	Particle 1		Particle 2		Bond	1	2	SRP
1400	0.92	0.82	0.96	0.92	0.64	0.85	0.93	0.11E-10
	1.01	1.16	1.01	1.06	0.86	1.11	1.03	0.20E-10
	0.72	0.77	1.11	1.06	0.57	0.74	1.08	0.78E-11
	1.01	1.06	1.11	1.06	0.96	1.03	1.08	0.40E-10
Mean								1.97E-11
1500	1.00	1.00	1.10	1.00	0.60	1.00	1.03	0.66E-11
	1.00	1.10	1.50	1.50	0.68	1.03	1.50	0.72E-11
	1.30	1.40	1.20	1.20	0.81	1.34	1.20	1.02E-11
	1.10	1.10	0.90	0.90	0.66	1.10	0.90	0.92E-11
Mean								0.82E-11
1600	1.48	1.48	1.48	1.39	1.02	1.48	1.42	1.60E-11
	1.30	1.39	1.02	1.02	0.79	1.33	1.02	1.16E-11
	0.74	0.84	1.02	1.02	0.65	0.77	1.02	1.34E-11
Mean								1.36E-11
1700	0.93	0.93	0.83	0.83	0.45	0.93	0.84	0.38E-11
	1.86	1.76	1.34	1.34	0.83	1.79	1.34	0.78E-11
	1.34	1.34	1.34	1.24	0.92	1.34	1.27	1.46E-11
Mean								0.86E-11
1800	2.60	2.60	0.87	0.87	0.75	2.60	0.87	1.02E-11
	1.54	1.54	1.35	1.35	1.02	1.54	1.35	1.64E-11
	1.73	1.73	0.77	0.77	0.42	1.73	0.77	0.26E-11
	1.16	1.25	0.87	0.87	0.69	1.19	0.87	1.06E-11
	0.96	0.87	0.77	0.77	0.51	0.90	0.77	0.60E-11
Mean								0.92E-11

APPENDIX C

(FORTRAN PROGRAMS)

The pages following contain the listing of the two FORTRAN programs, SRP10 and SRP20, which were used to numerically calculate the Sintering Rate Parameter.
Also included is a sample input/output sheet and a list of sample outputs from both programs.

```
C     PROGRAM FOR FINDING SINTERING RATE PARAMETER (SURFACE
C     TENSION/VISCOSITY) BASED ON THEORY BY J. FRENKEL FOR
C     ELLIPSOIDS ROTATED ABOUT MAJOR AXES AND TOUCHING ON ENDS
C     OF MAJOR AXES
C
C     INPUTS FOR THE PROGRAM:
C
C     LENGTH OF MAJOR AXIS FOR BOTH ELLIPSOIDS
C     LENGTH OF MINOR AXIS FOR BOTH ELLIPSOIDS
C     RADIUS OF THE BOND
C     TIME OF SINTERING
C     TIME STEP
C
C     *****DEFINE VARIABLES********
C
      REAL MAJO1, MAJO2, MINO1, MINO2, RADY
      REAL DT, DY, DR1, DR2, TIMET
      REAL ECC1, ECC2, THET1, THET2
      REAL RSTEP1, RSTEP2, YSTEP, XSTEP1, XSTEP2, TIME
      REAL DTHET1, DTHET2, DX1, DX2
      REAL DSURF1, DSURF2
      REAL FRWK1, FRWK2, GAMMA1, GAMMA2
      REAL SRP
C
      INTEGER COUNT
C
      PARAMETER (PI=3.1415927)
C
C     *****INPUT MODULE*******
C
      WRITE(6,*)'MAJOR AXIS OF FIRST ELLIPSOID?'
      READ(5,*)MAJO1
      WRITE(6,*)'MINOR AXIS OF FIRST ELLIPSOID?'
      READ(5,*)MINO1
      WRITE(6,*)'MAJOR AXIS OF SECOND ELLIPSOID?'
      READ(5,*)MAJO2
      WRITE(6,*)'MINOR AXIS OF SECOND ELLIPSOID?'
      READ(5,*)MINO2
      WRITE(6,*)'LENGTH OF BOND RADIUS?'
      READ(5,*)RADY
      WRITE(6,*)'TIME FOR SINTERING PROCESS?'
      READ(5,*)TIMET
      WRITE(6,*)'TIME STEP FOR CALCULATIONS?'
      READ(5,*)DT
C
C     *****CALCULATE RATE OF CHANGE FOR BOND RADIUS***
C     *****AND ELLIPSE RADII******
C
      DX1=(SQRT(MAJO1**2-(RADY**2*MAJO1**2/MINO1**2))-
     MAJO1)/TIMET
      DX2=(SQRT(MAJO2**2-(RADY**2*MAJO2**2/MINO2**2))-
```

```
     MAJO2)/TIMET
C
C
C     *****CALCULATE ECCENTRICITY FOR BOTH ELLIPSOIDS********
C
      ECC1=SQRT(MAJO1**2 - MINO1**2) / MAJO1
      ECC2=SQRT(MAJO2**2 - MINO2**2) / MAJO2
C
C     *****INITIALIZE PARAMETERS********
C
      RSTEP1=MAJO1
      RSTEP2=MAJO2
      THET1=0.
      THET2=0.
      YSTEP=0.
      XSTEP1=MAJO1
      XSTEP2=MAJO2
      COUNT=1
      TIME=0
C
C     *****MAIN PROGRAM******
C
      WHILE(YSTEP .LT. RADY)
C
C           ***CALCULATE RATE OF CHANGE OF X DIRECTION***
C           ***LENGTH AND OF THETA***
C
            XSTEP1=XSTEP1+(DT*DX1)
            XSTEP2=XSTEP2+(DT*DX2)
            YSTEP=(MINO1/MAJO1)*SQRT(MAJO1**2-XSTEP1**2)
            DY=((-MINO1/MAJO1)*XSTEP1*DX1)/
     A           SQRT(MAJO1**2-XSTEP1**2)
            DR1=(XSTEP1*DX1+YSTEP*DY)/
     A           SQRT(XSTEP1**2+YSTEP**2)
            DR2=(XSTEP2*DX2+YSTEP*DY)/
     A           SQRT(XSTEP2**2+YSTEP**2)
            RSTEP1=SQRT(XSTEP1**2+YSTEP**2)
            RSTEP2=SQRT(XSTEP2**2+YSTEP**2)
            DTHET1=(RSTEP1*DY-YSTEP*DR1)/
     A           (RSTEP1**2*SQRT(1+(YSTEP/RSTEP1)**2))
            DTHET2=(RSTEP2*DY-YSTEP*DR2)/
     A           (RSTEP2**2*SQRT(1+(YSTEP/RSTEP2)**2))
            THET1=ASIN(YSTEP/RSTEP1)
            THET2=ASIN(YSTEP/RSTEP2)
C
C           ***CALCULATE THE CHANGE IN SURFACE AREA***
C           ****OF ELLIPSOIDS*****
C
C           ***IF EITHER ELLIPSOID IS A SPHERE...***
C
            IF(ECC1 .NE. 0)THEN
```

```
                DSURF1=-(((DX1*PI*MINO1/MAJO1**2)
     A                  *SQRT(MAJO1**4+(MINO1**2-
     A                  MAJO1**2)*XSTEP1**2))+((DX1*PI*
     A                  MINO1*XSTEP1**2*(MINO1**2-
     A                  MAJO1**2))/(MAJO1**2*SQRT
     A                  (MAJO1**4+(MINO1**2-MAJO1**2)*
     A                  XSTEP1**2)))+((DX1*PI*MINO1)/(SQRT
     A                  (1-(ECC1**2*XSTEP1**2
     A                  /MAJO1**2))))
           ELSE
                DSURF1=2*PI*RSTEP1**2*
     A                  THET1*DTHET1
           END IF
C
           IF(ECC2 .NE. 0)THEN
                DSURF2=-(((DX2*PI*MINO2/MAJO2**2)
     A                  *SQRT(MAJO2**4+(MINO2**2-
     A                  MAJO2**2)*XSTEP2**2))+((DX2*PI*
     A                  MINO2*XSTEP2**2*(MINO2**2-
     A                  MAJO2**2))/(MAJO2**2*SQRT
     A                  (MAJO2**4+(MINO2**2-MAJO2**2)*
     A                  XSTEP2**2)))+((DX2*PI*MINO2)/(SQRT
     A                  (1-(ECC2**2*XSTEP2**2
     A                  /MAJO2**2))))
           ELSE
                DSURF2=2*PI*RSTEP2**2*
     A                  THET2*DTHET2
           END IF
C
C          ***CALCULATE VELOCITY GRADIENT & WORK****
C          ***OF FRICTION FORCES DIVIDED BY VISCOSITY***
C
           GAMMA1=DX1/MAJO1
           GAMMA2=DX2/MAJO2
           FRWK1=(8*PI/3)*MAJO1*MINO1**2*GAMMA1**2
           FRWK2=(8*PI/3)*MAJO2*MINO2**2*GAMMA2**2
C
C          ****CALCULATE SINTERING RATE PARAMETER*****
C
           SRP=(FRWK1+FRWK2)/(DSURF1+DSURF2)
C
C          ****BOOKKEEPING****
C
           TIME=TIME+DT
C
C          ****PRINT OUTPUT*****
  10       FORMAT(' ', 1X, I3, 6X, F7.1, 6X, E10.3, 6X, E10.3,
     A     6X, E10.3)
          WRITE(6,10) COUNT, TIME, SRP
     COUNT=COUNT+1
     END DO
```

```
WRITE(6,*)'PROGRAM COMPLETED'
PAUSE
STOP
END
```

```
C     PROGRAM FOR FINDING SINTERING RATE PARAMETER (SURFACE
C     TENSION/VISCOSITY) BASED ON THEORY BY J. FRENKEL FOR TWO
C     ELLIPSOIDS ROTATED ABOUT MINOR AXES AND TOUCHING ON ENDS
C     OF MINOR AXES
C
C     INPUTS FOR THE PROGRAM
C
C     LENGTH OF MAJOR AXIS FOR BOTH ELLIPSOIDS
C     LENGTH OF MINOR AXIS FOR BOTH ELLIPSOIDS
C     RADIUS OF THE BOND
C     TIME OF SINTERING
C     TIME STEP
C
C     *****DEFINE VARIABLES********
C
      REAL MAJO1, MAJO2, MINO1, MINO2, RADY
      REAL DT, DY, DR1, DR2, TIMET
      REAL ECC1, ECC2, THET1, THET2
      REAL RSTEP1, RSTEP2, YSTEP, XSTEP1, XSTEP2, TIME
      REAL DTHET1, DTHET2, DX1, DX2
      REAL DSURF1, DSURF2
      REAL FRWK1, FRWK2, GAMMA1, GAMMA2
      REAL SRP, RC1, RC2
C
      INTEGER COUNT
C
      PARAMETER (PI=3.1415927)
C
C     *****INPUT MODULE*******
C
      WRITE(6,*)'MAJOR AXIS OF FIRST ELLIPSOID?'
      READ(5,*)MAJO1
      WRITE(6,*)'MINOR AXIS OF FIRST ELLIPSOID?'
      READ(5,*)MINO1
      WRITE(6,*)'MAJOR AXIS OF SECOND ELLIPSOID?'
      READ(5,*)MAJO2
      WRITE(6,*)'MINOR AXIS OF SECOND ELLIPSOID?'
      READ(5,*)MINO2
      WRITE(6,*)'LENGTH OF BOND RADIUS?'
      READ(5,*)RADY
      WRITE(6,*)'TIME FOR SINTERING PROCESS?'
      READ(5,*)TIMET
      WRITE(6,*)'TIME STEP FOR CALCULATIONS?'
      READ(5,*)DT
C
C     *****CALCULATE RATE OF CHANGE FOR BOND RADIUS AND
C     *****ELLIPSE RADII******
C
      DX1=(SQRT(MINO1**2-(RADY**2*MINO1**2/MAJO1**2))-
     A MINO1)/TIMET
      DX2=(SQRT(MINO2**2-(RADY**2*MINO2**2/MAJO2**2))-
```

```
     A MINO2)/TIMET
C
C
C     *****CALCULATE ECCENTRICITY FOR BOTH ELLIPSOIDS********
C
      ECC1=SQRT(MAJO1**2 - MINO1**2) / MAJO1
      ECC2=SQRT(MAJO2**2 - MINO2**2) / MAJO2
C
C     *****INITIALIZE PARAMETERS********
C
      RSTEP1=MINO1
      RSTEP2=MINO2
      THET1=0.
      THET2=0.
      YSTEP=0.
      XSTEP1=MINO1
      XSTEP2=MINO2
      COUNT=1
      TIME=0
C
C     *****MAIN PROGRAM******
C
      WHILE(YSTEP .LT. RADY)
C
C           ***CALCULATE RATE OF CHANGE OF X DIRECTION***
C           ***LENGTH AND OF THETA***
C
            XSTEP1=XSTEP1+(DT*DX1)
            XSTEP2=XSTEP2+(DT*DX2)
            YSTEP=(MAJO1/MINO1)*SQRT(MINO1**2-XSTEP1**2)
            DY=((-MAJO1/MINO1)*XSTEP1*DX1)/
     A           SQRT(MINO1**2-XSTEP1**2)
            DR1=(XSTEP1*DX1+YSTEP*DY)/
     A           SQRT(XSTEP1**2+YSTEP**2)
            DR2=(XSTEP2*DX2+YSTEP*DY)/
     A           SQRT(XSTEP2**2+YSTEP**2)
            RSTEP1=SQRT(XSTEP1**2+YSTEP**2)
            RSTEP2=SQRT(XSTEP2**2+YSTEP**2)
            DTHET1=(RSTEP1*DY-YSTEP*DR1)/
     A           (RSTEP1**2*SQRT(1+(YSTEP/RSTEP1)**2))
            DTHET2=(RSTEP2*DY-YSTEP*DR2)/
     A           (RSTEP2**2*SQRT(1+(YSTEP/RSTEP2)**2))
            THET1=ASIN(YSTEP/RSTEP1)
            THET2=ASIN(YSTEP/RSTEP2)
C
C           ***CALCULATE THE CHANGE IN SURFACE AREA OF
C           ***ELLIPSOIDS*****
C
C           ***IF EITHER ELLIPSOID IS A SPHERE...***
C
            IF(ECC1 .NE. 0)THEN
```

```
C
                RC1=SQRT(MINO1**4+(MAJO1**4-
     A          MINO1**4)*XSTEP1**2)
C
                DSURF1=-((PI*XSTEP2**2*MAJO1*(MAJO1**2-
     A               MINO1**2)/
     A               (MINO1**2*RC1))+(PI*MAJO1*RC1/MINO1**2)
     A               +(PI*MINO1**2/ECC1)*((MAJO1**2-MINO1**2)
     A               *XSTEP1+MAJO1*ECC1*RC1)/(
     A               RC1**2+MAJO1*ECC1*XSTEP1*RC1))*DX1
          ELSE
                DSURF1=2*PI*RSTEP1**2*
     A               THET1*DTHET1
          END IF
C
          IF(ECC2 .NE. 0)THEN
C
                RC2=SQRT(MINO2**4+(MAJO2**4-
     A          MINO2**4)*XSTEP2**2)
C
                DSURF2=-((PI*XSTEP2**2*MAJO2*(MAJO2**2-
     A               MINO2**2)/
     A               (MINO2**2*RC2))+(PI*MAJO2*RC2/MINO2**2)
     A               +(PI*MINO2**2/ECC2)*((MAJO2**2-MINO2**2)
     A               *XSTEP2+MAJO2*ECC2*RC2)/(
     A               RC2**2+MAJO2*ECC2*XSTEP2*RC2))*DX2
          ELSE
                DSURF2=2*PI*RSTEP2**2*
     A               THET2*DTHET2
          END IF
C
C         ***CALCULATE VELOCITY GRADIENT & WORK OF FRICTION
C         FORCES DIVIDED BY VISCOSITY***
C
          GAMMA1=DX1/MINO1
          GAMMA2=DX2/MINO2
          FRWK1=(8*PI/3)*MINO1*MAJO1**2*GAMMA1**2
          FRWK2=(8*PI/3)*MINO2*MAJO2**2*GAMMA2**2
C
C         ****CALCULATE SINTERING RATE PARAMETER*****
C
          SRP=(FRWK1+FRWK2)/(DSURF1+DSURF2)
C
C         ****BOOKKEEPING****
C
          TIME=TIME+DT
C
C         ****PRINT OUTPUT*****
   10     FORMAT(' ', 1X, I3, 6X, F7.1, 6X, E10.3, 6X, E10.3,
     A     6X, E10.3)
         WRITE(6,10) COUNT, TIME, SRP
```

```
COUNT=COUNT+1
END DO
WRITE(6,*)'PROGRAM COMPLETED'
PAUSE
STOP
END
```

SAMPLE INPUT/OUTPUT OF SRP10 FORTRAN PROGRAM

```
MAJOR AXIS OF FIRST ELLIPSOID?
50E-6
MINOR AXIS OF FIRST ELLIPSOID?
50E-6
MAJOR AXIS OF SECOND ELLIPSOID?
50E-6
MINOR AXIS OF SECOND ELLIPSOID?
50E-6
LENGTH OF BOND RADIUS?
5E-6
TIME FOR SINTERING PROCESS?
3600
TIME STEP FOR CALCULATIONS?
600
     1           600.0          0.930E-10
     2          1200.0          0.930E-10
     3          1800.0          0.932E-10
     4          2400.0          0.934E-10
     5          3000.0          0.934E-10
     6          3600.0          0.936E-10
PROGRAM COMPLETED
```

Table C-4.1 Sample results of SRP10 FORTRAN Program

***All calculations were made using a 3600 second sintering period with 600 second time steps.

***Dimensions are in micrometers.

Major Radius	Minor Radius	Major Radius	Minor Radius	Bond Radius	SRP Value	Frenkel Equation
50	50	50	50	5	0.94E-10	0.93E-10
50.1	49.9	50.1	49.9	5	0.93E-10	0.93E-10
50	50	50	50	20	0.18E-09	0.15E-09
50.1	49.9	50.1	49.9	20	0.16E-09	0.15E-09
**55	45	55	45	5	1.26E-10	0.96E-10
**60	40	60	40	5	1.72E-10	1.01E-10
65	35	65	35	5	0.24E-09	NA
50	50	49	49	5	0.95E-10	NA
50.1	50.1	49.9	49.9	5	0.94E-10	NA
55	55	50	50	5	0.89E-10	NA
60	60	45	45	5	0.91E-10	NA
70	70	40	40	5	0.92E-10	NA
50	50	40	40	5	0.11E-09	NA
50	50	40	40	10	0.44E-10	NA
50	50	40	40	25	0.37E-10	NA

**Average Radius use in Frenkel's Equation.

Table C-4.2 Sample results of SRP20 FORTRAN Program

***All calculations were made using a 3600 second sintering period with 600 second time steps.

***Dimensions are in micrometers.

Major Radius	Minor Radius	Major Radius	Minor Radius	Bond Radius	SRP Value	Frenkel Equation
50	50	50	50	5	0.94E-10	0.93E-10
50.1	49.9	50.1	49.9	5	0.92E-10	0.93E-10
50	50	50	50	20	0.18E-09	0.15E-09
50.1	49.9	50.1	49.9	20	0.15E-09	0.15E-09
**55	45	55	45	5	0.68E-10	0.96E-10
**60	40	60	40	5	0.47E-10	1.01E-10
65	35	65	35	5	0.32E-10	NA
50	50	49	49	5	0.95E-10	NA
50.1	50.1	49.9	49.9	5	0.94E-10	NA
55	55	50	50	5	0.89E-10	NA
60	60	45	45	5	0.91E-10	NA
70	70	40	40	5	0.92E-10	NA
50	50	40	40	5	0.11E-09	NA
50	50	40	40	10	0.44E-10	NA
50	50	40	40	25	0.37E-10	NA

**Average Radius used in Frenkel's Equation.

APPENDIX D

(DERIVATION OF FRENKEL'S MODEL)

DERIVATION OF FRENKEL'S MODEL

Consider two identical spherical particles, initially of radius a_o. After contact, the radius of the particles is a, except for the portion of the interface. (Figure A-4.1 and Figure A-4.2)

Since the volume of the system is constant, we can determine a geometric relationship between a and a_o.

Upon examination of one of the particles shown in Figure A-4.2, it is seen that the volume of the particle can be expressed as

$$\frac{4}{3}\pi a^3 - V_c \qquad (1)$$

where V_c is the volume of the contact interface.

The volume of V_c can be found in a math handbook or calculated by using solid angles, and becomes, after substitution,

$$V_c = \frac{\pi}{6}(a - a\cos\theta)\left[3a^2\sin^2\theta + (a - a\cos\theta)^2\right]. \qquad (2)$$

Expanding and simplifying,

$$V_c = \frac{\pi a}{6}(1 - \cos\theta)(3a^2\sin^2\theta + a^2 - 2a^2\cos\theta + a^2\cos^2\theta)$$

$$V_c = \frac{\pi a^3}{6}(1 - \cos\theta)(3\sin^2\theta + 1 - 2\cos\theta + \cos^2\theta).$$

Since $\sin^2\theta + \cos^2\theta = 1$,

$$V_c = \frac{\pi a^3}{6}(1 - \cos\theta)(2\sin^2\theta + 2 - 2\cos\theta)$$

$$V_c = \frac{\pi a^3}{3}\left(1 - \cos\theta\right)\left(\sin^2\theta + 1 - \cos\theta\right)$$

$$V_c = \frac{\pi a^3}{3}\left(\sin^2\theta + 1 - \cos\theta - \sin^2\theta\cos\theta + \cos^2\theta - \cos\theta\right)$$

$$V_c = \frac{\pi a^3}{3}\left(2 - 2\cos\theta - \sin^2\theta\cos\theta\right)$$

$$V_c = \frac{\pi a^3}{3}\left[2 - 2\cos\theta - \left(1 - \cos^2\theta\right)\cos\theta\right]$$

$$V_c = \frac{\pi a^3}{3}\left(2 - 3\cos\theta + \cos^3\theta\right). \qquad (3)$$

Since volume of the system remains constant, we can express this as:

$$\frac{4}{3}\pi a_o^3 = \frac{4}{3}\pi a^3 - V_c \qquad (4)$$

or, by substituting, expanding, and simplifying,

$$\frac{4}{3}\pi a_o^3 = \frac{4}{3}\pi a^3 - \frac{2\pi a^3}{3} - \frac{\pi a^3}{3}\left(-3\cos\theta + \cos^3\theta\right)$$

$$\frac{4}{3}\pi a_o^3 = \frac{2}{3}\pi a^3 - \frac{\pi a^3}{3}\left(-3\cos\theta + \cos^3\theta\right)$$

$$\frac{4}{3}\pi a_o^3 = \frac{\pi a^3}{3}\left(2 + 3\cos\theta - \cos^3\theta\right).$$

Solving for *a* gives:

$$a^3 = \frac{4a_o^3}{\left(2 + 3\cos\theta - \cos^3\theta\right)}$$

$$a = \frac{4^{\frac{1}{3}}\, a_o}{\left(2 + 3\cos\theta - \cos^3\theta\right)^{\frac{1}{3}}}. \qquad (5)$$

Now the surface area of the system can be determined by: Total surface area = 2(Surface area of spheres) - 2(Surface of contact area for each sphere), or

$$S_T = 2S - 2S_c$$

$$S_T = 2(4\pi a^2) - 2S_c. \quad (6)$$

Again using a math manual, the formula for S_c, becomes, after substitution,

$$S_c = \pi(2a)(a - a\cos\theta)$$

$$S_c = 2\pi a^2(1 - \cos\theta)$$

$$S_c = 2\pi a^2 - 2\pi a^2 \cos\theta. \quad (7)$$

Substituting the expression for S_c into (6) gives

$$S_T = 8\pi a^2 - 4\pi a^2 + 4\pi a^2 \cos\theta$$

$$S_T = 4\pi a^2 + 4\pi a^2 \cos\theta. \quad (8)$$

In order to find work of surface tension forces per unit time, we need to know how the difference in surface area changes with time, which can be expressed by

$$\frac{d\Delta S}{dt} = \frac{dS_T}{dt} - \frac{dS_o}{dt} \quad (9)$$

where S_o is original surface area given by $S_o = 2(4\pi a_o^2)$. Since S_o is a constant, its derivative is zero, therefore

$$\frac{d\Delta S}{dt} = \frac{dS_T}{dt}. \quad (10)$$

Taking the derivative of S_T, we obtain

$$\frac{dS_T}{dt} = 8\pi a \frac{da}{dt} + 8\pi a \cos\theta \frac{da}{dt} - 4\pi a^2 \sin\theta \frac{d\theta}{dt}. \quad (11)$$

Recalling the expression for *a*,

$$a = 4^{\frac{1}{3}} a_o(2 + 3\cos\theta - \cos^3\theta)^{\frac{-1}{3}},$$

then

$$\frac{da}{dt} = \left(-4^{\frac{1}{3}}\right) a_o\left(\frac{1}{3}\right)(2 + 3\cos\theta - \cos^3\theta)^{\frac{-4}{3}} \left(-3\sin\theta + 3\cos^2\theta \sin\theta\right) \frac{d\theta}{dt}$$

$$\frac{da}{dt} = \left(-4^{\frac{1}{3}}\right) a_o(2 + 3\cos\theta - \cos^3\theta)^{\frac{-4}{3}} \left(-\sin\theta + \cos^2\theta \sin\theta\right) \frac{d\theta}{dt}$$

$$\frac{da}{dt} = \left(4^{\frac{1}{3}}\right)a_o(2 + 3\cos\theta - \cos^3\theta)^{\frac{-4}{3}} \left(\sin\theta - \left(1-\sin^2\theta\right)\sin\theta\right) \frac{d\theta}{dt}$$

$$\frac{da}{dt} = \left(4^{\frac{1}{3}}\right)a_o(2 + 3\cos\theta - \cos^3\theta)^{\frac{-4}{3}} \left(\sin\theta - \sin\theta + \sin^3\theta\right) \frac{d\theta}{dt}$$

$$\frac{da}{dt} = \left(4^{\frac{1}{3}}\right)a_o(2 + 3\cos\theta - \cos^3\theta)^{\frac{-4}{3}} \left(\sin^3\theta\right) \frac{d\theta}{dt}. \qquad (12)$$

Now, substitution into the expression for dS_T/dt gives

$$\frac{dS_T}{dt} = \left(8\pi a - 8\pi a \cos\theta\right)\left[4^{\frac{1}{3}} a_o\left(2+3\cos\theta-\cos^3\theta\right)^{\frac{-4}{3}} \sin^3\theta\right]\frac{d\theta}{dt} - 4\pi a^2 \sin\theta \frac{d\theta}{dt}$$

and, assuming small angles, $\sin\theta = \theta$ and $\cos\theta = 1$ results in

$$\frac{dS_T}{dt} = \left(8\pi a - 8\pi a\right)\left[4^{\frac{1}{3}} a_o(2+3-1)^{\frac{-4}{3}} \theta^3\right]\frac{d\theta}{dt} - 4\pi a^2 \theta \frac{d\theta}{dt}.$$

The first term vanishes and leaves

$$\frac{dS_T}{dt} = -4\pi a^2\theta \frac{d\theta}{dt}. \qquad (13)$$

Recalling the expression for a and substituting gives

$$\frac{dS_T}{dt} = -(4\pi)\left(\frac{\left(4^{\frac{2}{3}}\right)a_o^2}{\left(2+3\cos\theta-\cos^3\theta\right)^{\frac{2}{3}}}\right)\theta \frac{d\theta}{dt}.$$

Again, using small angle theory,

$$\frac{dS_T}{dt} = -4\pi a_o^2\theta \frac{d\theta}{dt}. \qquad (14)$$

Substituting into (10), we obtain

$$\frac{d\Delta S}{dt} = -4\pi a_o^2\theta \frac{d\theta}{dt}. \qquad (15)$$

Now the rate of work done by surface tension forces can be expressed as

$$W = -\sigma \frac{d\Delta S}{dt} \qquad (16)$$

$$W = \sigma \, 4\pi a_o^2 \theta \frac{d\theta}{dt} \qquad (17)$$

where σ is surface tension.

In Frenkel's model, the rate of work done by surface tension forces is assumed to be equivalent to the rate of energy dissipation by viscous action. Frenkel also seemed to assume that the flow was incompressible, that there was only one velocity defined in the problem (that of the interface as it moved toward the center of the drop), and that the viscous dissipation due to dilatation dominates the shear dissipation. The expression for viscous dissipation per unit volume, in spherical coordinates, is

$$\phi = 2\mu \left\{ \left(\frac{\partial v_r}{\partial r} \right)^2 + \left(\frac{1}{r} \frac{\partial v_\theta}{\partial \theta} + \frac{v_r}{r} \right)^2 + \left(\frac{1}{r \sin\theta} \frac{\partial v_\varphi}{\partial \varphi} + \frac{v_r}{r} + \frac{v_\theta \cot\theta}{r} \right)^2 \right\}$$
$$+ \mu \left\{ \left[r \frac{\partial}{\partial r} \left(\frac{v_\theta}{r} \right) + \frac{1}{r} \frac{\partial v_r}{\partial \theta} \right]^2 + \left[\frac{1}{r \sin\theta} \frac{\partial v_r}{\partial \varphi} + r \frac{\partial}{\partial r} \left(\frac{v_\varphi}{r} \right) \right]^2 \right\}$$
$$+ \mu \left\{ \left[\frac{\sin\theta}{r} \frac{\partial}{\partial \theta} \left(\frac{v_\varphi}{\sin\theta} \right) + \frac{1}{r \sin\theta} \frac{\partial v_\theta}{\partial \varphi} \right]^2 \right\} . \qquad (18)$$

As mentioned earlier, Frenkel only accounted for viscous dissipation due to dilatation. After discarding all other negligible terms, the expression for ϕ is simply

$$\phi = 2\mu \left(\frac{\partial v_r}{\partial r}\right)^2, \qquad (19)$$

and the expression for Φ, the rate of viscous dissipation for the entire system, becomes

$$\Phi = 2\left(\frac{4}{3}\pi a_o^3\right)\phi$$

$$\Phi = \frac{16}{3}\pi a_o^3 \mu \left(\frac{\partial v_r}{\partial r}\right)^2. \qquad (20)$$

Now, equating the rate of work of surface forces to the rate of energy dissipation,

$$\Phi = -\sigma \frac{d\Delta S}{dt}, \qquad (21)$$

or, by changing from partial derivatives and substituting,

$$\frac{16}{3}\pi a_o^3 \mu \left(\frac{dv_r}{dr}\right)^2 = \sigma 4\pi a_o^2 \theta \frac{d\theta}{dt}.$$

Simplifying, we obtain

$$\frac{4}{3} a_o \mu \left(\frac{dv_r}{dr}\right)^2 = \sigma\theta \frac{d\theta}{dt}. \qquad (22)$$

The next objective is the evaluation of the differential quantity in (22) that represents the velocity gradient. If we denotes the position of the contact surface by *z*, then dz/dt is the velocity of the contact surface relative to the center of the drops.

$$z = a \cos\theta \qquad (23)$$

$$\frac{dz}{dt} = -a \sin\theta \frac{d\theta}{dt} + \cos\theta \frac{da}{dt} \qquad (24)$$

Substituting earlier expressions for a and da/dt:

$$\frac{dz}{dt} = -\frac{4^{\frac{1}{3}}\, a_o \sin\theta \frac{d\theta}{dt}}{(2+3\cos\theta-\cos^3\theta)^{\frac{1}{3}}} + \frac{4^{\frac{1}{3}}\, a_o \cos\theta \sin^3\theta \frac{d\theta}{dt}}{(2+3\cos\theta-\cos^3\theta)^{\frac{4}{3}}}.$$

Again, using small angle theory,

$$\frac{dz}{dt} = -\frac{4^{\frac{1}{3}}\, a_o\, \theta \frac{d\theta}{dt}}{(2+3-1)^{\frac{1}{3}}} + \frac{4^{\frac{1}{3}}\, a_o\, \theta^3 \frac{d\theta}{dt}}{(2+3-1)^{\frac{4}{3}}}.$$

Also, for small angles, $\theta^3 \approx 0$, so

$$\frac{dz}{dt} = -a_o\, \theta \frac{d\theta}{dt}. \qquad (25)$$

But we are interested in the velocity gradient, so

$$\frac{dv_r}{dr} = \frac{v_r}{r} = \frac{\frac{dz}{dt}}{z}$$

and, since $z \approx a_o$ by the small angle assumption,

$$\frac{dv_r}{dr} = -\theta\frac{d\theta}{dt}. \qquad (26)$$

Substituting into (22) and rearranging,

$$\frac{4}{3}a_o\mu \left(\theta\frac{d\theta}{dt}\right)^2 = \sigma\theta\frac{d\theta}{dt}$$

$$\frac{4}{3}a_o\mu\, \theta\frac{d\theta}{dt} = \sigma$$

$$\theta\frac{d\theta}{dt} = \frac{3\sigma}{4a_o\mu}$$

$$\theta\, d\theta = \frac{3\sigma}{4a_o\mu}\, dt. \qquad (27)$$

Integrating gives

$$\frac{\theta^2}{2} = \frac{3\sigma}{4a_o\mu}\, t + \text{Constant}$$

$$\theta^2 = \frac{3\sigma}{2a_o\mu} t + C.$$

Initial conditions demand that $\theta=0$ at $t=0$; therefore $C=0$, and

$$\theta^2 = \frac{3\sigma}{2a_o\mu} t. \qquad (28)$$

We now relate θ to y by

$$\sin \theta = \frac{y}{a}. \qquad (29)$$

We can see from (5) that, in the limit of small angles, $a \approx a_o$; therefore,

$$\sin \theta = \frac{y}{a_o}. \qquad (30)$$

Also, in the limit of small angles, $\sin \theta = \theta$; therefore,

$$y = a_o\theta \Rightarrow \theta = \frac{y}{a_o}. \qquad (31)$$

Substituting this expression into (28) gives

$$\left(\frac{y}{a_o}\right)^2 = \frac{3\sigma t}{2a_o\mu}$$

$$y^2 = \frac{3a_o\sigma t}{2\mu} = \frac{3a\sigma t}{2\mu},$$

which is the final form of Frenkel's equation.

VITA

John Alan Howlett, a native of Lincoln County, Tennessee, was born in Huntsville, Alabama on August 6, 1970. He attended high school at Triana Village Baptist School, Huntsville, where he received his diploma in June, 1988. The following September he commenced his collegiate study in Mechanical Engineering at Pensacola Christian College, Pensacola, Florida. After receiving his Bachelor of Science degree in May, 1992, he entered the University of Tennessee Space Institute, Tullahoma, where he was also employed as a research assistant in the Magnetohydrodynamics Energy Conversion Programs. He received his Masters of Science degree from the University of Tennessee in May, 1994. Not only does John Alan Howlett acknowledge without apology the lordship of an Almighty God Who spoke the universe into existence, but he also anticipates the blessings promised by this God, Who cannot lie, which He related to all men in the Biblical passages of Deuteronomy 7 and John 3:

> "Know therefore that the LORD thy God, He is God, the faithful God, which keepeth covenant and mercy with them that love Him and keep His commandments to a thousand generations; and repayeth them that hate Him to their face, to destroy them: He will not be slack to him that hateth Him, He will repay him to his face."
>
> "For God so loved the world, that He gave His only begotten Son, that whosoever believeth in Him should not perish, but have everlasting life."

Thanks be to God for His unspeakable gift!